A Measurement of the Branching Ratio of the Decay of the τ Lepton to Five Charged Hadrons

by

Laura Stumpf

B.Sc., University of Victoria, 1996.
A Thesis Submitted in Partial Fulfillment of the
Requirements for the Degree of
MASTER OF SCIENCE
in the Department of Physics and Astronomy.

We accept this thesis as conforming
to the required standard.

Dr. R. Sobie, Co-Supervisor (Department of Physics and Astronomy)

Dr. R. Keeler, Co-Supervisor (Department of Physics and Astronomy)

Dr. M. Lefebvre, Departmental Member (Department of Physics and Astronomy)

Dr. D. M. Miller, Outside Member (Department of Computer Science)

Dr. D. Axen, External Examiner (University of British Columbia)

Supervisors: Dr. R. Sobie, Dr. R. Keeler

Abstract

The branching ratio of the decay of the τ lepton to five charged hadrons, $B(\tau^- \longrightarrow 3\mathrm{h}^- 2\mathrm{h}^+ (\geq 0\pi^0)\nu_\tau)$, has been measured with the OPAL detector at LEP using data collected between 1991 and 1995. The branching ratio was measured to be

$$B(\tau^- \longrightarrow 3\mathrm{h}^- 2\mathrm{h}^+ (\geq 0\pi^0)\nu_\tau) = (1.25 \pm 0.14 \pm 0.08) \times 10^{-3}$$

where the first error is statistical and the second is systematic.

Examiners:

Dr. R. Sobie, Co-Supervisor (Department of Physics and Astronomy)

Dr. R. Keeler, Co-Supervisor (Department of Physics and Astronomy)

Dr. M. Lefebvre, Departmental Member (Department of Physics and Astronomy)

Dr. D. M. Miller, Outside Member (Department of Computer Science)

Dr. D. Axen, External Examiner (University of British Columbia)

Contents

List of Tables

List of Figures

Acknowledgements

I thank Randy Sobie who does a remarkable job as supervisor and mentor, and my children for their support, encouragement, and belief in me. I also thank the other members of the UVIC High Energy Physics group for making a lively, congenial working environment.

Chapter 1

Introduction

All of the complicated interactions that are observed in the universe are combinations of four underlying, fundamental forces: strong, weak, electromagnetic, and gravitational, each of which involves the exchange of a particular fundamental particle[1]. Through the study of these interactions, one attempts to reduce the complexities of the macroscopic world to its most basic properties.

One of the ways in which this is done is by studying the behaviour of fundamental particles. Fundamental particles include the particles that mediate the interactions mentioned above, and also quarks and leptons which are the basic constituents of matter. While quarks are not observed individually, they do combine to form baryons (three bound quarks) and mesons (bound states consisting of a quark and an antiquark) which are collectively known as hadrons. Protons and neutrons are examples of baryons, while pions ($\pi^{\pm}$, π^0) are examples of mesons.

Leptons include electrons, e^-, muons, μ^-, tau particles, τ^-, and their associated neutrinos, ν_e, ν_μ, ν_τ. The electron is the lightest charged lepton with a mass of $m_e = 5.11 \times 10^{-4}$ GeV.[2] The muon mass is $m_\mu = 0.106$ GeV; it decays to an electron

---

[1]A fundamental particle is one with no observed substructure.

[2]In this work, the convention $\hbar = c = 1$ will be used.

and two neutrinos with a lifetime of 2.19703×10^{-6} seconds [1]. The τ is the heaviest lepton, with a mass of $m_\tau = 1.78$ GeV [2]; it is the only lepton which is kinematically allowed to decay to hadrons[3] in addition to decaying into lighter leptons with a lifetime of 290.0×10^{-15} seconds [1]. The neutrinos have been assumed to be massless; however, recent evidence suggests that they may have non-zero but small masses [3].

Precise measurements of the branching ratios of the different decay modes of the τ can provide information about the strong, weak, and electromagnetic forces. The branching ratio is defined to be the fraction of particles that decay via a particular decay mode. In this thesis, a measurement of the branching ratio of tau decay to five charged hadrons with or without a neutral pion, $B(\tau^- \longrightarrow 3h^- 2h^+ (\geq 0\pi^0)\nu_\tau)$, is presented. This rare decay mode of the τ has a branching ratio of approximately 0.001, and is not as well understood as the more common decay modes; for example, it is not known whether this τ decay mode proceeds through intermediate resonances, i.e. very short-lived particles. Further information about this decay mode is important because, for example, the kinematics of this decay have been used to determine one of the current upper limits on the mass of the τ neutrino (for example, see [4]). A non-zero neutrino mass could be partly responsible for the missing mass (dark matter) in the universe [5]. Chapter 2 provides a brief description of the Standard Model of Particle Physics, the decay width of the τ lepton, and its relationship to the branching ratio.

The τ leptons used in this work were created at the Large Electron Positron (LEP) colliding beam synchrotron at CERN[4] near Geneva, Switzerland via the reaction $e^+e^- \to Z^0 \to \tau^+\tau^-$. At LEP, electron and positron beams are accelerated around an

---

[3]The hadrons in this case are most likely to be pions or kaons.

[4]European Organisation for Nuclear Research

underground ring and are made to collide in four separate interaction areas, one of which houses the OPAL[5] detector. Chapter 3 describes LEP and the OPAL detector.

Chapter 4 describes the selection of $e^+e^- \rightarrow \tau^+\tau^-$ events and Chapter 5 describes the selection of $\tau^- \longrightarrow 3\text{h}^-2\text{h}^+(\geq 0\pi^0)\nu_\tau$ decays. Chapter 6 presents the branching ratio calculation and the systematic errors. Chapter 7 compares these results with those from other experiments, and summarizes this work.

---

[5]**O**mni-**P**urpose **A**pparatus for **L**ep

Chapter 2

Theory

2.1   The Standard Model

The properties of fundamental particles and their interactions are described by the Standard Model of Particle Physics [6]. This model has had notable success in predicting measurable quantities such as cross sections, lifetimes, and branching ratios.

The fundamental particles of which matter is composed are fermions (particles with half-integer spin). In particular, quarks and leptons are spin-$\frac{1}{2}$ particles which interact with each other via the exchange of fundamental bosons (particles with integer spin). Each of the fundamental forces has its own exchange particle which mediates the interaction. At the subatomic scales studied to date, the gravitational force has no measurable effects and can be neglected. The mediating bosons, shown in Table 2.1, are the photons, $W^\pm$ and Z^0 particles, and gluons for the electromagnetic, weak, and strong forces, respectively.

Force	Mediating boson
Electromagnetic	photons
Strong	gluons
Weak	$W^\pm/Z^0$

Table 2.1: Exchange particles for the fundamental forces.

The six flavours of quarks and leptons are arranged into three generations, as shown in Table 2.2. The table is divided horizontally into generations; for example, the e^- and ν_e leptons together with the u and d quarks form the first generation. Each particle has an associated antiparticle with opposite electric charge.

Leptons			Quarks		
Flavour	Charge	Mass(GeV)	Flavour	Charge	Mass
ν_e	0	$< 15 \times 10^{-9}$	u	$+\frac{2}{3}$	1.5 - 5 MeV
e	-1	5.11×10^{-4}	d	$-\frac{1}{3}$	3 - 9 MeV
ν_μ	0	$< 1.7 \times 10^{-4}$	c	$+\frac{2}{3}$	1.1 - 1.4 GeV
μ	-1	0.106	s	$-\frac{1}{3}$	60 - 170 MeV
ν_τ	0	$< 18 \times 10^{-3}$	t	$+\frac{2}{3}$	173.8 ± 5.2 GeV
τ	-1	1.78	b	$-\frac{1}{3}$	4.1 - 4.4 GeV

Table 2.2: Some properties of the fundamental constituents of matter in the Standard Model. Electric charge is given in units of positron charge. The masses given are the Particle Data Book 1998 evaluations [1].

The electromagnetic force affects all charged particles. A graphic representation of the fundamental interaction between these particles is shown in the Feynman diagram in Figure 2.1(a), where a fermion interacts with an electromagnetic field by the exchange of a virtual photon. Both quarks and charged leptons interact electromagnetically; however, only quarks can interact via the strong force. Figure 2.1(b) shows a quark interacting with the strong field via the exchange of a gluon. All fundamental fermions interact via the weak force. Figure 2.1(c) illustrates the form of a charged weak interaction, where a charged lepton l^- interacts with the weak field via the exchange of a W^-. As a result, the outgoing lepton is neutral (ν_l). Quarks may also interact via the charged weak force through a flavour-changing process; this is illustrated in Figure 2.1(d). The basic form of the neutral weak interaction is shown in Figure 2.1(e), where f stands for any fundamental fermion. The neutral leptons

only interact via the weak force.

The form of the coupling between fermions is theoretically predicted by the gauge invariance of the Standard Model, i.e. there exists a group of symmetry operations or local gauge transformations under which the measurable quantities remain invariant. For example, it is possible to exchange the colour of the quarks in an interaction without changing any of the physics. The rules for interchanging the properties are specified by a gauge group.

The Standard Model is based on a combination of three gauge groups, $SU_c(3) \times SU_L(2) \times U_Y(1)$. The couplings between strongly interacting particles by the exchange of gluons is described by $SU_c(3)$. The other two groups, $SU_L(2) \times U_Y(1)$, together describe the unified electroweak interaction. In nature, the invariance of the unified electroweak group is not evident because of a process known as "spontaneous symmetry breaking". The coupling strengths of the weak force corresponding to $SU_L(2)$ which proceeds via exchange of the W and Z particles, and that of the electromagnetic force in which a photon is exchanged, are measured separately.

2.2 Properties of the Tau Particle

The τ is a third generation lepton, differing from the other charged leptons only in its mass which allows for hadronic decays as well as leptonic ones. The τ decay modes are categorised into either leptonic or semi-leptonic (those including hadrons) decays and are represented by Feynman diagrams as shown in Figure 2.2.

In the semi-leptonic decay, the τ decays to a ν_τ and hadrons where the hadrons will most likely be pions or kaons. In order to conserve charge, the τ must decay to an odd number of charged hadrons. About 85 percent of τ's decay to one charged particle (1-prong), 15 percent to three charged particles (3-prong), and 0.1 percent
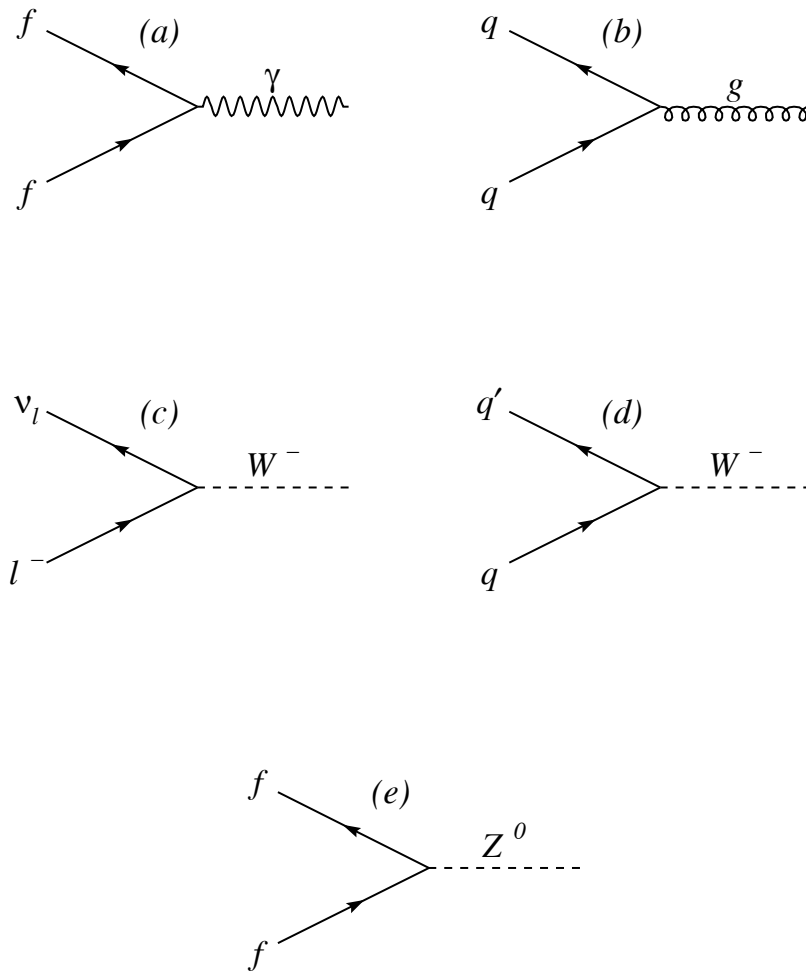
Figure 2.1: Electromagnetic (a), strong (b), charged weak (c,d), and neutral weak (e) processes.

to five charged particles (5-prong). Some examples of these are shown in Table 2.3.

Decay mode	Branching ratio
$\tau^- \to e^- \nu_\tau \bar{\nu}_e$	(0.1781 ± 0.0007)
$\tau^- \to \mu^- \nu_\tau \bar{\nu}_\mu$	(0.1737 ± 0.0009)
$\tau^- \to h^- (\geq 0 \text{ neutrals}) \nu_\tau$	(0.4952 ± 0.0016)
$\tau^- \to h^- h^- h^+ (\geq 0 \text{ neutrals}) \nu_\tau$	(0.1518 ± 0.0013)
$\tau^- \to h^- h^- h^- h^+ h^+ (\geq 0 \text{ neutrals}) \nu_\tau$	(0.00097 ± 0.00007)

Table 2.3: Some of the decay modes of the τ, with branching ratio values from the 1998 Particle Data Book [1]. Here, $h^\pm$ stands for $\pi^\pm$ or $K^\pm$, and *neutrals* means any neutral hadron whose decay products include γ's and/or π^0's.

2.2.1 The Decay Width

The partial decay width is proportional to the transition rate of the particle from the initial state to a particular final state. In general, a partial decay width can be expressed as

$$dΓ = \frac{|M|^2}{2m} dLips \tag{2.1}$$

where $dLips$ is the Lorentz invariant phase space factor and m is the mass of the decaying particle. In the case of a 6-body decay such as $\tau^- \to 3h^- 2h^+ \nu_\tau$, we have

$$dLips = \left[\prod_{i=1}^{6} \frac{d^3 \mathbf{p}_i}{(2\pi)^3 2E_i} \right] (2\pi)^4 \delta^4 (p_\tau - p_1 - p_2 - p_3 - p_4 - p_5 - p_6). \tag{2.2}$$

The p_i's ($\mathbf{p}_i$)'s are the four-vector (three-vector) momenta of the six decay particles shown in Figure 2.2(b) and the E_i's are the corresponding energies.

The matrix element M takes into account the dynamics of the process such as the strength of the coupling between particles; the phase space factor corresponds to kinematic constraints such as conservation of 4-momentum. The matrix element for the leptonic τ decays is well understood; however, the matrix element for the
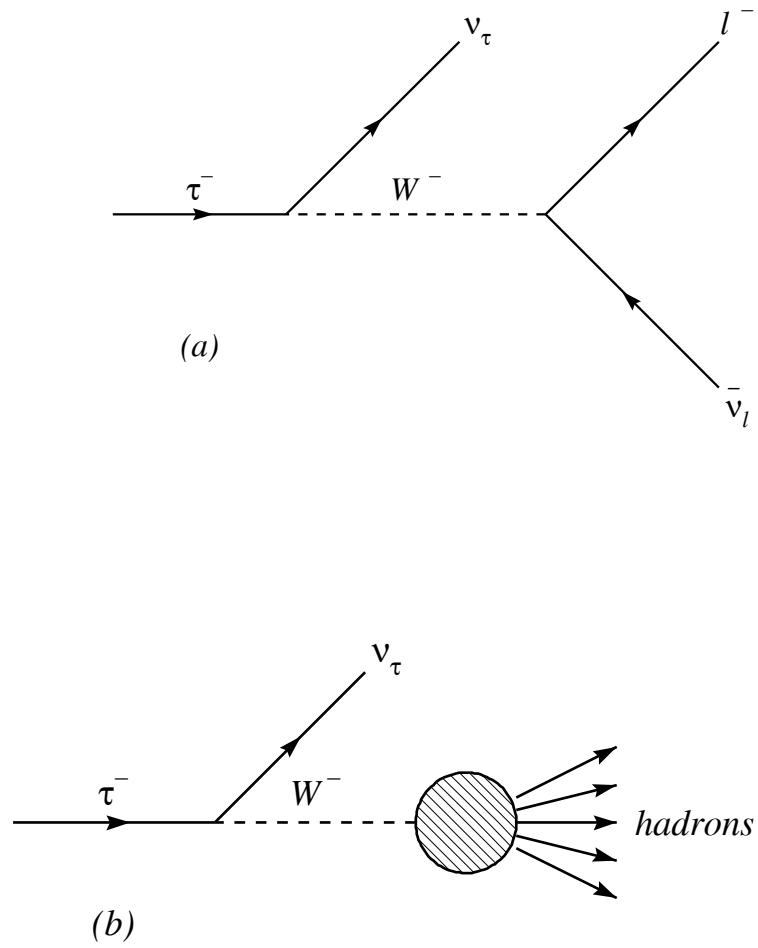
Figure 2.2: Leptonic (a) and semi-leptonic (b) τ decay. The blob signifies our ignorance of the hadronization process.

semi-leptonic τ decays is complicated by the hadronization process, and is discussed in the next section.

2.2.2   Semi-leptonic τ Decay Width

For semi-leptonic decays of the τ, the matrix element has the following form:

$$M = \frac{-g_w}{2\sqrt{2}\,M_W^2}[\bar{u}_{\nu_\tau}\gamma_\mu(1-\gamma_5)u_\tau]J^\mu \tag{2.3}$$

where J^μ represents the hadronic current. At a more fundamental level, the W decays into quarks which hadronize to form pions and kaons. There is no method for directly calculating the contribution from this current.

The term $\gamma_\mu(1-\gamma_5)$ in Equation 2.3 corresponds to the vector and axial vector components of the weak charged current. The weak charged current has the following properties [7]:

	Isospin	G-parity (G)	Spin$^{\text{Parity}}$
Vector	1	+1	1^-
Axial-vector	1	-1	0^-, 1^+

G-parity is defined to be charge conjugation followed by a rotation in isospin space about the I_2 axis, i.e.

$$G = CR_2. \tag{2.4}$$

For multipion final states we have

$$G|n\pi> = (-1)^n|n\pi>. \tag{2.5}$$

Final states with an odd number of pions will be negative G-parity eigenstates, and those with even numbers of pions will be positive G-parity eigenstates. As as result, semi-leptonic τ decays in general can be subdivided into vector decays if there is an

even number of pions in the final state, and axial-vector decays if there is an odd number of pions in the final state.

Axial-vector Decays

In the situation where the hadronization produces a single pion (Figure 2.3), the hadronic current becomes $J^\mu = f_\pi p^\mu$ where p^μ is the four-vector of the pion, and f_π is the pion decay constant. The same $W \to \pi$ vertex occurs both in the decay $\tau^- \to \pi^- \nu_\tau$ and in pion decay $\pi \to \mu \bar{\nu}_\mu$. A value of $f_\pi = 131.74$ MeV is calculated from the measurement of the pion lifetime [7]. The partial decay width for the reaction $\tau^- \to \pi^- \nu_\tau$ can be written

$$d\Gamma = \frac{G_F^2 f_\pi^2 \cos^2 \theta_C}{16 \pi M_\tau} \left(M_\tau^2 - M_\pi^2 \right)^2 , \tag{2.6}$$

where θ_C is the Cabibbo angle, and G_F, given by

$$G_F = \frac{\sqrt{2}}{8} \left(\frac{g_w}{M_W} \right)^2 \tag{2.7}$$

is the Fermi coupling constant.

The matrix element of the $\tau^- \to 2\pi^- \pi^+ \nu_\tau$ axial-vector three pion decay mode has been predicted by Kühn and Santamaria [8] and Isgur, Morningstar, and Reader [9]. The decay is assumed to proceed through the $a_1(1270)$ resonance which subsequently decays to a $\rho\pi$ state. This decay has been studied by a number of experiments and is found to be reasonably well-modelled by the theoretical predictions (see for example [10]).

There is only one calculation of the $\tau^- \to 3\pi^- 2\pi^+ \nu_\tau$ five pion decay current by Pham [11], who estimated the branching ratio to be of the order of 0.01.
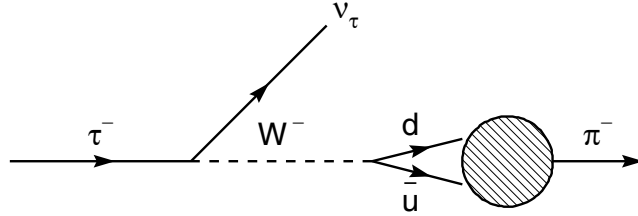
Figure 2.3: $\tau^- \to \pi^- \nu_\tau$ decay.

Vector Decays

It is possible to use the conserved vector current (CVC) hypothesis to theoretically calculate the branching ratios for the vector decays. In the case of $\tau^- \to \rho^- \nu_\tau$[1], Tsai [12] comments that "CVC is equivalent to the statement that the coupling of W to ρ is obtainable from the $\gamma\rho$ coupling". More generally, $\tau^- \to W \to (n\pi)^- \nu_\tau$ decays can be related to $e^+ e^- \to \gamma \to n\pi$ if n is even. For example, the $\tau^- \to \pi^- \pi^0 \nu_\tau$ branching ratio can be calculated using the I=1 part of the $e^+ e^- \to \pi^+ \pi^-$ cross section [13]. Similarly, the $\tau^- \to (4\pi)^- \nu_\tau$ branching ratio can be obtained from the $e^+ e^- \to 4\pi$ cross section. The $\tau^- \to (6\pi)^- \nu_\tau$ branching ratio cannot be determined as there are no $e^+ e^- \to 6\pi$ data available.

2.2.3   The Branching Ratio

The branching ratio for a particular mode of decay can be expressed as a ratio of the appropriate partial width to the total width. In this thesis, we are interested in the

---

[1]The two pion decay is dominated by the ρ resonance.

branching ratio

$$B\left(\tau^- \longrightarrow 3\mathrm{h}^-2\mathrm{h}^+(\geq 0\pi^0)\nu_\tau\right) = \frac{\Gamma\left(\tau^- \longrightarrow 3\mathrm{h}^-2\mathrm{h}^+(\geq 0\pi^0)\nu_\tau\right)}{\Gamma_\tau}. \qquad (2.8)$$

The total width Γ_τ in the denominator of Equation 2.8 is the inverse of the lifetime. The partial width in the numerator must be found using the transition rate described in section 2.2.1.

Chapter 3

The OPAL Experiment

This chapter describes the experimental facility which created the τ particles used in this analysis, and the detector used to identify them.

3.1 The LEP collider

The LEP collider is a facility consisting of several particle accelerators which work in stages to produce and store electrons and positrons, and collide them at high energies.

The collider has two main sections: the injector chain, which produces, stores, and accelerates electrons and positrons to 20 GeV, and the main (LEP) ring which accelerates them to approximately 45 GeV, thereby providing the centre-of-mass energy of approximately 90 GeV needed for Z^0 production.

Figure 3.1 shows the injector chain and the LEP ring. Positrons are produced by bombarding the converter target with 200 MeV electrons from a linac. The electrons and positrons are then accelerated in another linac (LIL) to 600 MeV, after which they are collected in the Electron Positron Accumulator (EPA). They are subsequently injected in bunches, or pulsed, into the Proton Synchrotron (PS) where their energy is increased to 3.5 GeV, and then are transferred to the Super Proton Synchrotron (SPS) where they are accelerated to 20 GeV. The final stage of the process occurs in

the LEP ring, where they are accelerated to 45 GeV.

The LEP collider is operated in eight bunch mode, in which the electron and positron beams are injected into the LEP ring as eight equally spaced bunches. Prior to 1992, four bunch mode was used. Each bunch has approximately 4×10^{11} particles and completes a revolution in 8.9×10^{-5} seconds. The beams are made to collide in four interaction areas, one of which houses the OPAL detector as mentioned in the introduction. The positions of the other detectors, ALEPH[1], L3[2], and DELPHI[3] are shown on Figure 3.1.

3.2   The OPAL Detector

The OPAL detector is a solenoidal magnetic spectrometer composed of three main parts: the central tracking system, the electromagnetic calorimeter, and the hadron calorimeter and muon chambers [14]. Figure 3.2 is a schematic diagram of OPAL. The central tracking system and the electromagnetic calorimeter will be described in some detail, whereas the hadron calorimeter and muon chambers were not pertinent to this analysis and will be described briefly.

OPAL is a cylindrical detector, co-axial to a beam pipe with radius 5.35 cm (see Figure 3.2). The coordinate system is defined such that the x-axis is horizontal, with $+x$ pointing toward the centre of LEP, the y-axis is vertical, and the $+z$-axis is in the direction of motion of the electron beam. The origin of the coordinate system is located at the interaction point in the centre of the detector. The polar angle θ is measured from the $+z$-axis; the azimuthal angle ϕ is measured from the $+x$-axis

---

[1]**A**pparatus for **LE**P **P**hysics

[2]**LEP 3** experiment

[3]**D**etector with **L**epton **P**hoton and **H**adron **I**dentification
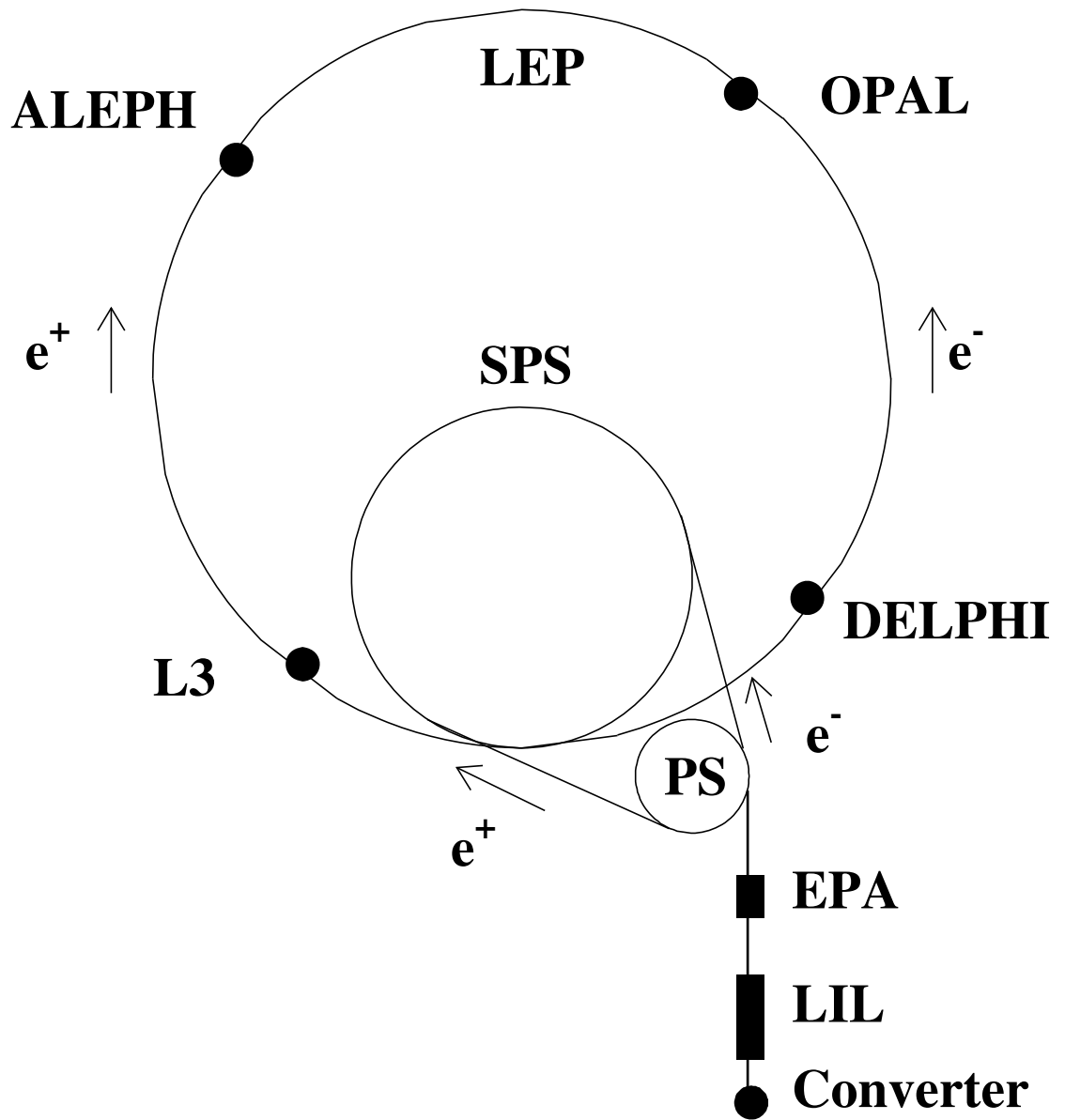
Figure 3.1: Schematic view of the injection scheme and the LEP ring, along with the locations of the four experimental areas.

ELECTROMAGNETIC
CALORIMETERS

HADRON
CALORIMETERS

FORWARD
DETECTOR

MUON CHAMBERS

TIME OF FLIGHT
AND PRESAMPLER

Z CHAMBERS

JET CHAMBER

VERTEX CHAMBER

OPAL-ENSEMBLE EN PERSPECTIVE
KLW 06.1990
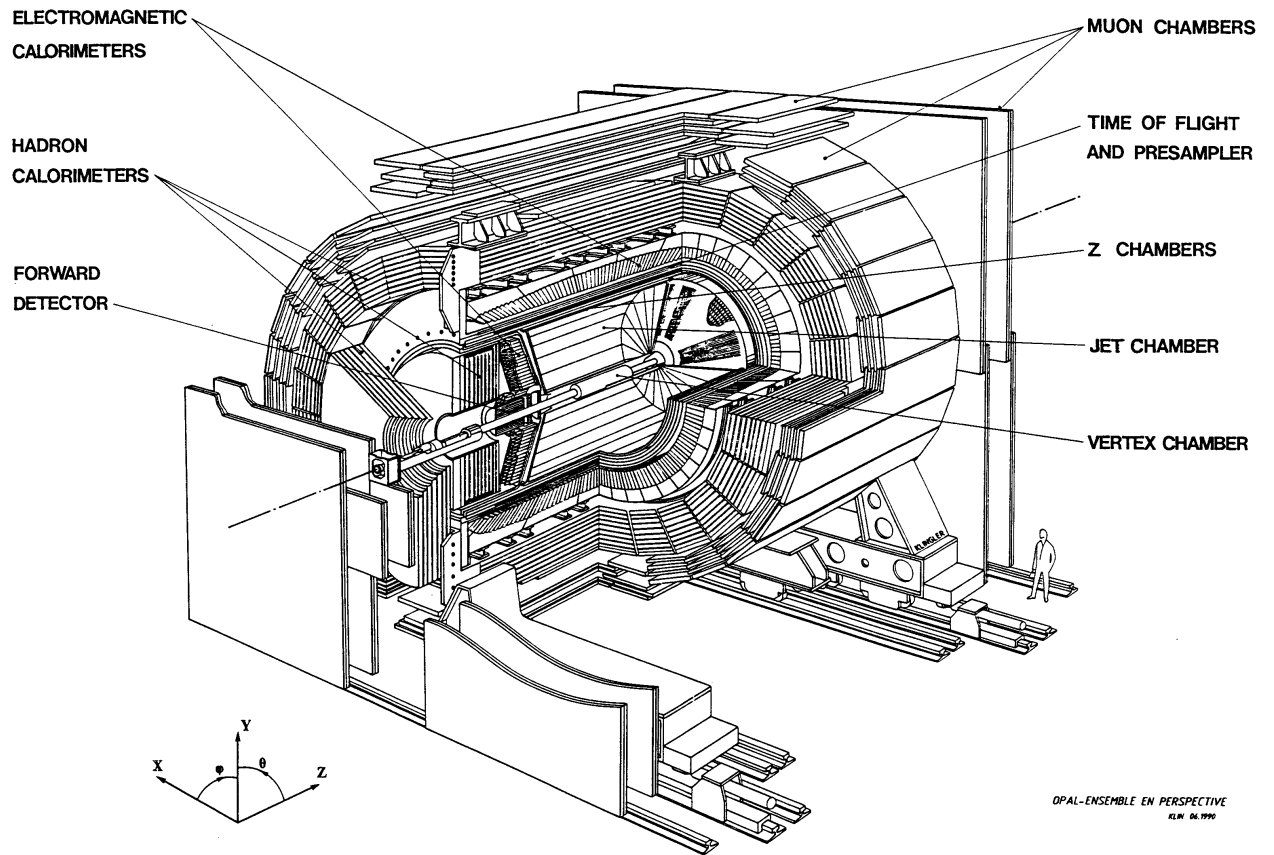
Figure 3.2: A cut away view of the OPAL detector showing its main components. The electron beam runs along the $+z$ axis and the $+x$ axis points to the centre of the LEP ring.

about the z-axis. The barrel region is the central portion of the detector, covering approximately $|\cos\theta| \leq 0.81$, and the endcap region extends from the barrel region to $|\cos\theta| \leq 0.98$. The detectors in the endcap region were not used in this analysis and will not be discussed. The detector description begins at the vacuum beam pipe and proceeds radially outward.

3.2.1   The Central Tracking System

The central tracking system includes a Silicon Microvertex Detector, followed by a pressure vessel holding the central vertex detector, jet chamber, and Z-chambers. The pressure vessel is held at a pressure of four bars, and is surrounded by a solenoidal magnet which provides a magnetic field of 0.435 T. The function of the central tracking system is to provide information which makes it possible to reconstruct the trajectories (tracks) of charged particles traversing the detector and to determine their momentum.

Silicon Microvertex Detector

The innermost detector is the Silicon Microvertex Detector (SI), which consists of two barrels of double-sided Silicon Microstrip Detectors at radii of 6 and 7.5 cm [15, 16]. The inner layer consists of 11 "ladders" arranged azimuthally around the beam pipe, and the outer layer consists of 14 ladders. The ladders overlap to avoid gaps in the ϕ coverage. Each ladder consists of three silicon wafers daisy-chained together. Each wafer is a pair of single-sided silicon detectors 33 mm wide and 60 mm long glued back-to-back. One side has readout strips running longitudinally (in the z direction) in order to measure the ϕ position, while the other side has readout strips running azimuthally in order to measure the z position.

A charged particle entering the silicon detector causes a current to flow, which is measured by electronic equipment at the end of each ladder. SI has a track position resolution of 10 μm in ϕ and 15 μm in z, and helps to pinpoint the location of the primary vertex, the point at which the e^+e^- collision occurred.

Central Vertex Detector

The 1 m long Central Vertex Detector (CV) is the first of the detectors within the pressure vessel and extends from the inner wall of the pressure vessel (at a radius of 8.8 cm) to a radius of 23.5 cm. It consists of an inner axial region and an outer stereo region, each divided into 36 sectors in ϕ. The sectors of the inner region each contain a plane of 12 sense wires strung parallel to the beam and ranging radially outwards from 10.3 to 16.2 cm. The stereo sectors lie between radii of 18.8 and 21.3 cm, each containing a plane of 6 sense wires each of which is inclined at an angle of approximately 4° relative to the z-direction. A charged particle moving through the detector ionizes the gas. The resulting ions drift to the charged wires; a precise measurement of the drift time to the axial wires allows the $r - \phi$ position to be calculated to within 50μm [14]. The time difference of the signal's arrival at opposite ends of an axial wire provides an estimate of the z position which is used by the OPAL track trigger and in pattern recognition. An accurate z measurement is found by combining the information from the axial and the stereo sectors, which provides a resolution of 700μm.

Jet Chamber

The Central Jet Chamber (CJ) is a large volume cylindrical drift chamber 4 m long, with an inner radius of 25 cm and an outer radius of 185 cm. The chamber is divided into 24 identical sectors in ϕ. Each sector contains a sense wire plane extending

radially outwards with 159 anode wires strung parallel to the beam direction, and two cathode planes which form the boundaries between adjacent sectors [14]. The ionization of the gas caused by the passage of a charged particle results in charges being collected on the anode wires. The integrated charge collected is measured at each end of the wire; the ratio of these two measurements for a given wire determines the z position of the particle's track. The $r - \phi$ position is determined by the position of the wire and the drift time to the wire, respectively. This provides a resolution of 135 μm in $r - \phi$ and 6 cm in z [14].

The chamber is in a known magnetic field and hence the track curvature can be used to find the momentum of the particle. The resolution of momentum measurements was found to be

$$\frac{\sigma_p}{p^2} = 2.2 \times 10^{-3} \text{GeV}^{-1} \tag{3.1}$$

where momentum p is in GeV.

A particle loses energy as it ionizes the gas. The rate of energy loss, $\frac{dE}{dx}$, is a function of particle type (electrons, muons, pions, kaons, and protons) and is momentum dependent. It is measured using the total charge collected on the anode wires. The four bar pressure of the gas was chosen to optimize the $\frac{dE}{dx}$ measurement. Figure 3.3 shows the dependence of $\frac{dE}{dx}$ on momentum for the particle species listed above. The points are measured values which can be seen to be in good agreement with the theoretical expectation.

The Z-chambers

The last of the subdetectors within the pressure vessel, the Z-chambers (CZ) provide a precise measurement of the z position of particle tracks. They consist of 24 drift chambers, each 4 m long and divided in the z direction into eight cells. Each cell has
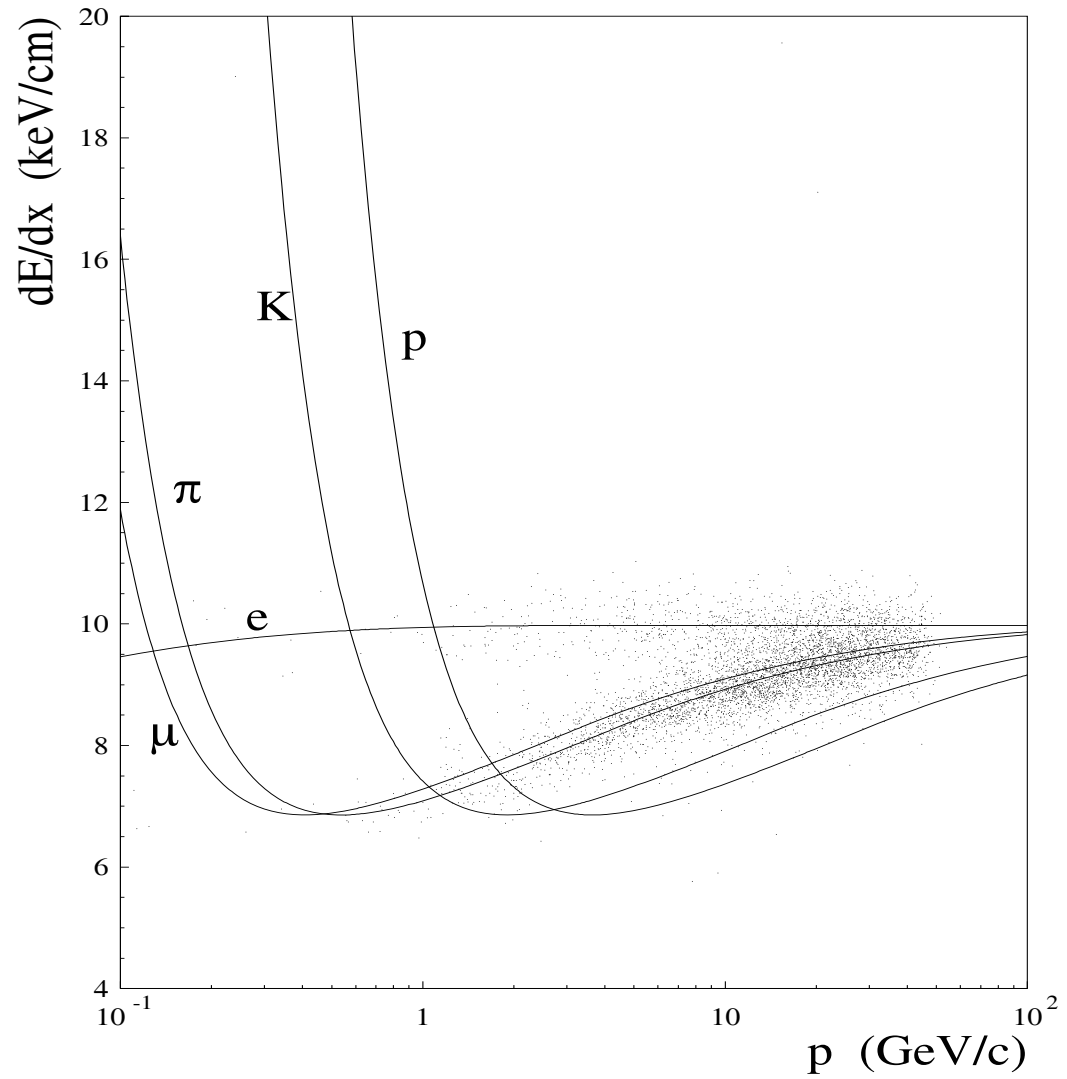
Figure 3.3: Ionization measurements $\left(\frac{dE}{dx}\right)$ for various particle species. Theory curves are overlaid with real data (points).

six anode wires running in the ϕ direction and placed at increasing radii. Measurements of the drift time to the wire, and the wire position give a z measurement with a resolution of 300 μm.

The Overall Tracking Resolution

The tracking system without SI provides a resolution of 75 μm in the $r - \phi$ plane and 2 mm in the $r - z$ plane [14]. With SI, the resolution of the impact parameter measurement is 15 μm in the $r - \phi$ plane, and resolution in the z direction is $20 - 50$ μm[16].

3.2.2   Solenoidal Magnet and Time of Flight Detector

Immediately outside the pressure vessel lies the magnet, which consists of a solenoidal coil and an iron yoke. The coil provides a uniform magnetic field of 0.435 T aligned with the electron beam and the magnetic flux is returned through the iron yoke.

The time-of-flight (TOF) system forms a barrel around the outside of the solenoid, consisting of 160 scintillation counters each 6.840 m long at a mean radius of 2.360 m. These are used to measure the time of flight of a particle from the interaction region, allowing for rejection of cosmic ray events. The barrel region of the TOF system (TB) is used in the OPAL trigger; a TOF signal within 50 ns of a known beam crossing time is required for a good event.

3.2.3   The Electromagnetic Calorimeter

The lead glass Electromagnetic Calorimeter (ECAL) measures the energies and positions of electrons, positrons and photons. A photon or electron is expected on average to lose all of its energy in ECAL, while a pion will lose about one-third of its energy.

Before entering the lead glass Electromagnetic Calorimeter, particles pass through approximately two radiation lengths[4] of material, due mostly to the solenoidal coil and the wall of the pressure vessel. Thus, most electromagnetic showers begin before the lead glass itself. To compensate for this, presamplers are installed immediately in front of the lead glass to measure the position and energy of these electromagnetic showers. The presampler is able to improve the electromagnetic energy resolution of a shower because the pulse height observed by the device is proportional to the number of charged particles entering it.

The barrel region of the presampler (PB) is at a radius of 2.388 m, and is made up of 16 wire chambers each having two layers of drift tubes containing wires that run parallel to the beam direction. The chambers are independently read out by cathode strips on both sides of each layer of tubes which are oriented at $45°$ to the wire direction to provide both ϕ and z positions [14].

The barrel region of the lead glass Electromagnetic Calorimeter (EB) consists of a cylindrical array of lead glass blocks of length 37 cm (equal to 24.6 radiation lengths), positioned at a radius of 2.455 m [14]. The longitudinal axes of the blocks point towards the interaction region. The area of the blocks transverse to the longitudinal direction is 10 cm $\times$ 10 cm. Each lead glass block is backed by a light guide, and then a phototube which detects the Čerenkov radiation produced in the glass by relativistic particles. The energy resolution of the lead glass calorimeter without any material in front was found to be $\sigma_E/E = 0.002 + 0.063 GeV^{\frac{1}{2}}/\sqrt{E}$, where E is measured in GeV [14]. However, the two radiation lengths of material in front of ECAL substantially degrades the energy resolution.

---

[4]A radiation length is the distance in which an electron's energy is reduced by a factor of e by bremsstrahlung radiation as it passes through a material.

3.2.4   The Hadron Calorimeter and Muon Chambers

Outside the electromagnetic calorimeter is the iron return yoke of the magnet, which provides four or more interaction lengths[5] of absorber. This is used as part of the Hadron Calorimeter (HCAL). The yoke is segmented into eight iron slabs, alternating with nine layers of wire detector chambers, from radii 3.39 to 4.39 m. Because of the 2.2 interaction lengths of material before the hadron calorimeter, the energy of a hadron will include a component in the ECAL as well as the HCAL. Essentially all hadrons will be absorbed at this stage, leaving only muons to pass on to the muon chambers [14].

Outside the HCAL are 110 large drift chambers arranged in four layers in the barrel region, which make up the barrel region of the muon calorimeter (MB). Each chamber is 1.2 m wide, and 90 mm deep. Muons are identified by matching tracks in the central tracking system with tracks in the muon chamber.

---

[5]An interaction length is the mean free path of a particle before undergoing a nuclear collision.

Chapter 4

Tau Selection

This chapter describes the data set and the simulated events used in this analysis, and then describes the selection of $e^+e^- \to \tau^+\tau^-$ events.

4.1   The Data Sets

Data taken during the 1991 to 1995 running periods of LEP are used in this analysis. The trigger identifies events of interest which are then recorded for further processing. Most subdetectors and other associated trigger hardware must be in good running order at the time of data-taking for the measurements to be used in the τ selection criteria. To this end, there are four status levels defined for each: 0 indicates that the status is unknown, 1 indicates that the unit is off, 2 indicates that the unit is partially operating (some subdetectors may have regions that no longer operate), and 3 means the subdetector or trigger is fully functioning. The minimum levels required for each subdetector and trigger used in the τ selection are shown in Table 4.1. If no requirement was placed on a particular trigger, the trigger status is left blank. The top line names the pertinent subdetector; the abbreviations are defined in the previous chapter except for EE which is the endcap region of the electromagnetic calorimeter, and HS which refers to hadron calorimeter strips.

25

	CV	CJ	TB	PB	EB	EE	HS	MB
Detector Status	3	3	3	2	3	3	3	3
Trigger Status		2			2	3		

Table 4.1: Detector and trigger status levels required in the τ selection.

Monte Carlo simulations of $e^+e^- \to \tau^+\tau^-$ events are used to determine efficiencies and backgrounds. A total of 975,000 Monte Carlo $e^+e^- \to \tau^+\tau^-$ events were generated using KORALZ, a Monte Carlo program which creates four-vector quantities [17]. Once the four-vector momenta of the τ's have been generated, the TAUOLA [18] program is called to simulate the decay of the τ's using the τ branching ratios. Although the branching ratios used in the simulations were the world averages at the time the Monte Carlo programs were created, in this work, the numbers of events are weighted to reflect the current world branching ratio averages wherever those averages for the background channels have changed in the intervening years.

The four-vectors produced by KORALZ and TAUOLA are then processed by the OPAL detector simulation program GOPAL [19], which uses the CERN library package GEANT [20] to simulate the detector's response to the Monte Carlo particles. After this stage of processing, the simulated detector responses are in exactly the same format as the OPAL data collected from LEP, and the simulated events are henceforth processed using the same reconstruction program (ROPE) as the data.

A total of 5,100,000 Monte Carlo $e^+e^- \to q\bar{q}$ events are produced in a similar manner using JETSET and HERWIG [21, 22].

4.2 Selection of $e^+e^- \to Z^0 \to \tau^+\tau^-$ Events

At LEP, the collisions between the electron and positron beams result in the production of Z^0 particles. The Z^0 can decay to charged lepton pairs (e^+e^-, $\mu^+\mu^-$,

$\tau^+\tau^-$), neutrino pairs ($\nu_e\bar{\nu}_e$, $\nu_\mu\bar{\nu}_\mu$, $\nu_\tau\bar{\nu}_\tau$), or quark pairs ($q\bar{q}$) which produce multi-hadron events. The branching ratio for each of these modes of decay is about 10.1 percent for the combined charged lepton channels, 20 percent for the combined neutrino channels, and 69.9 percent for the combined quark channels [1]. To begin the analysis, it is necessary to select the $\tau^+\tau^-$ events out of all the Z^0 decays.

The Z^0's are produced at rest, so that the $\tau^+\tau^-$ are produced with equal and opposite momenta. The mean lifetime of the τ is 290.0 $\pm$ 1.2 fs [1]; it travels an average distance of $\gamma c\tau_\tau = 2.24$ mm before decaying, hence most τ's decay inside the beam pipe. This results in a characteristic τ signature of two back-to-back sets of tracks (produced by the charged decay products) in the central detectors, which are matched with areas of activity in the electromagnetic calorimeter (produced by either charged or neutral decay particles). Further, the decay particles are boosted because the τ is highly relativistic, producing a collimated conical stream of decay particles, or jet. Figure 4.1 shows a typical 5-prong τ decay in OPAL.

The τ selection criteria place specific constraints on the properties of the tracks and the areas of ECAL activity (called ECAL clusters). These requirements ensure that the tracks and clusters are not from cosmic rays or interactions of the beams with atoms in the beam pipe. The requirements are shown in Table 4.2.

The standard OPAL τ pair selection criteria [23] are outlined in Tables 4.3 and 4.4. Each event is required to have two jets, each with at least one good charged track. The following algorithm is used to define a jet. The jet direction is initially set to the direction of the highest energy good track or ECAL cluster. The next highest energy good track or cluster within a cone of half-angle 35° is added to the first track, and the jet direction is redefined by the vector sum. The second step is repeated until there are no more tracks or clusters to add that fall within the cone.

Run:event 5074: 95081 Date 940517 Time 192653 Ctrk(N= 6 Sump= 78.0) Ecal(N= 10 SumE= 56.1) Hcal(N= 9 SumE= 9.0)
Ebeam 45.571 Evis 87.8 Emiss 3.4 Vtx (-.01,   .05,   .42) Muon(N= 0) Sec Vtx(N= 0) Fdet(N= 0 SumE= .0)
Bz=4.350 Thrust= .9991 Aplan= .0002 Oblat= .0098 Spher= .0005

Y
Z
X

200. cm.   510 20 50 GeV

Centre of screen is (.0000,   .0000,   .0000)
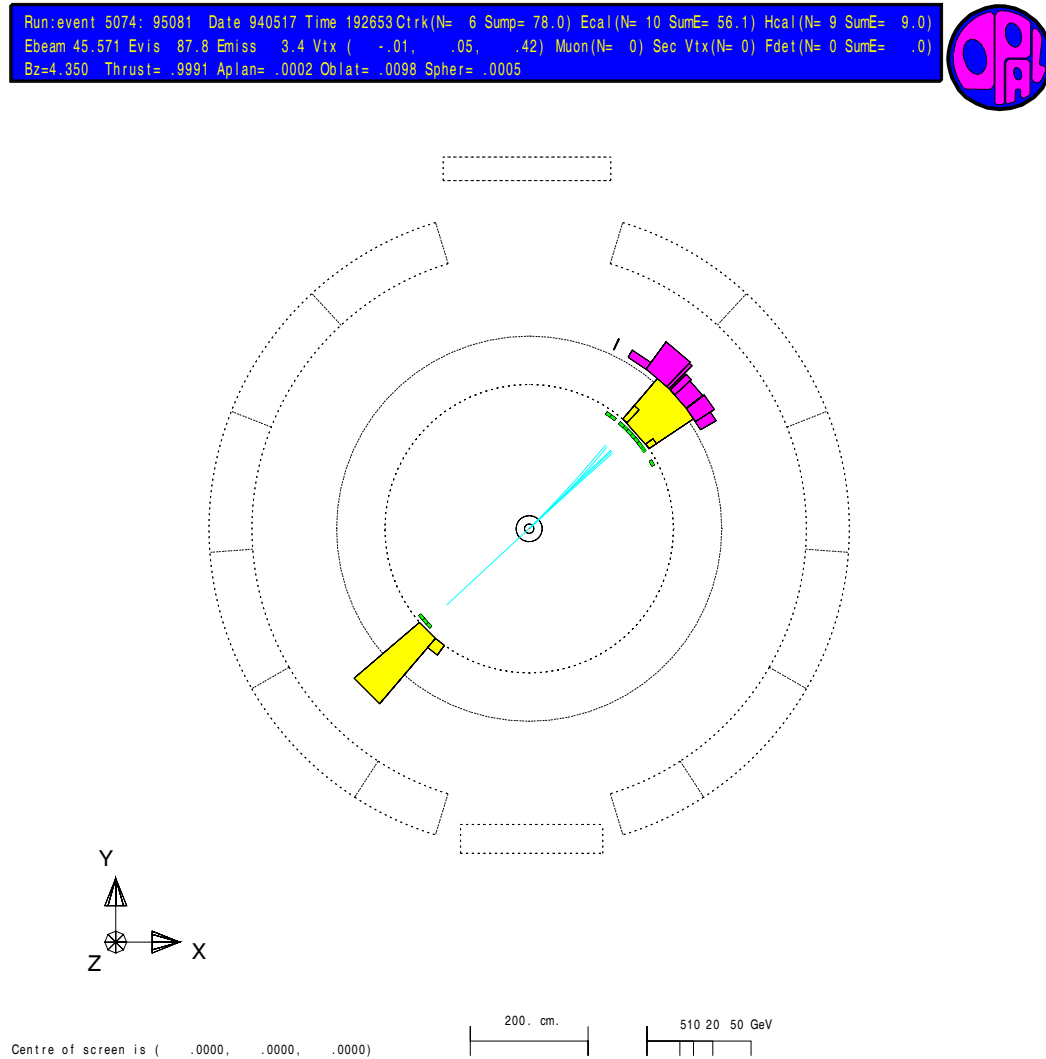
Figure 4.1: A typical OPAL event, showing a τ 1-prong jet and a τ 5-prong jet. The view is along the beam direction, showing the transverse plane. The concentric rings correspond to the outer edges of the beam pipe, vertex chamber, jet chamber, electromagnetic calorimeter, and hadron calorimeter. The rectangles in the electromagnetic calorimeter represent energy deposits with the rectangle height being proportional to the amount of energy deposited.

	Requirement	Variable definition
Good track definition	$N_{CJ}^{hits} \geq 20$	N_{CJ}^{hits}: number of hits in the jet chamber.
	$P_T \geq 0.1$ GeV	P_T: the momentum transverse to the beam direction.
	$|d_0| \leq 2$ cm	$|d_0|$: distance to the beam axis at the point of closest approach.
	$|z_0| \leq 75$ cm	$|z_0|$: track displacement along the beam axis from the interaction point.
Good Barrel ECAL cluster	$N_{blocks} \geq 1$	N_{blocks}: number of ECAL blocks in cluster.
	$E_{clusters} \geq 0.1$ GeV	$E_{clusters}$: total energy in cluster.

Table 4.2: Good charged track and ECAL cluster definitions for the τ pair selection.

The total measured energy in the event, which includes the scalar sum of the momenta of the good tracks and the total energy of the good clusters, must be at least 1 percent of the beam energy E_{beam}. The average value of $|\cos\theta|$ for the two jets must be less than 0.68, restricting the locations of the measurements to the barrel region of the detector.

The background from leptonic and multihadron events needs to be removed. These events have the following properties:

- Bhabha events $(e^+e^- \rightarrow e^+e^-)$ are characterised by back-to-back high energy charged particles which deposit almost the entire centre-of-mass energy in the ECAL. These are screened out by requiring τ pair candidates to have either $\Sigma E_{clusters} \leq 0.8 E_{CM}$ or $\Sigma E_{clusters} + 0.3\Sigma E_{track} \leq E_{CM}$; $\Sigma E_{clusters}$ is the total energy deposited in the ECAL, and ΣE_{track} is the total energy deposited in the jet chamber.

- Di-muon events $(e^+e^- \rightarrow \mu^+\mu^-)$ are characterised by back-to-back high energy charged particles, which deposit very little energy in the ECAL. These events are removed by matching activity in the muon chambers or hadronic calorime-

ter with tracks in the jet chamber, and then requiring that the total energy deposited in the jet chamber and the ECAL is less than $0.6E_{CM}$.

- Multihadron events $(e^+e^- \to q\bar{q})$ at the LEP energy are characterised by large track and cluster multiplicities. The τ pair selection removes these events by requiring the number of good charged tracks in the event to be between two and eight, and the number of good ECAL clusters to be less than or equal to 10.

Another type of background to the τ sample is two-photon events, $e^+e^- \to (e^+e^-)X$, where $X = e^+e^-$, $\mu^+\mu^-$, $\tau^+\tau^-$, or $q\bar{q}$. The e^+ and e^- are emitted at angles close to the beam and are often undetected, while the X represents particles that have relatively little energy, and large acolinearity.[1] These events are rejected by requiring the acolinearity to be less than $15°$, and the visible energy E_{vis} to be greater than 0.03 E_{CM}. The visible energy is the maximum of either the jet energy measured in the ECAL, or the jet energy measured in the jet chamber. Furthermore, if $E_{\text{vis}} \le 0.20E_{CM}$, then the event must have energy greater than 2.0 GeV deposited in either the jet chamber or the ECAL.

Additional criteria are also used to reject cosmic rays (see Table 4.4), using $|d_0|$ which is the minimum perpendicular distance between the reconstructed track and the interaction point, $|z_0|$ which is the minimum distance in the z direction between the reconstructed track and the interaction point, and TOF information.

After the τ selection, there are 98347 data events (196694 individual τ jets). The non-τ background in the sample is shown in Table 4.5 [24].

---

[1]The acolinearity between two vectors is $180°$ minus the angle between the vectors.

	Requirements	Variable definition
Good event	$N_{\mathrm{jet}} = 2$	N_{jet}: number of jets satisfying the total energy requirement.
	$\lvert\cos\theta\rvert < 0.68$	$\lvert\cos\theta\rvert$: average value of $\lvert\cos\theta\rvert$ for the two jets.
	$E_{\mathrm{jet}} \geq 0.01 E_{\mathrm{beam}}$	E_{jet}: total track and cluster energy in jet. E_{beam}: the energy of the LEP beam.
$e^+e^- \to e^+e^-$ rejection	$\Sigma E_{\mathrm{clusters}} \leq 0.8 E_{CM}$ or $\Sigma E_{\mathrm{clusters}} + 0.3\Sigma E_{\mathrm{track}} \leq E_{CM}$	E_{clusters} and E_{track}: energy of ECAL clusters and charged tracks in event.
$e^+e^- \to \mu^+\mu^-$ rejection	$\sum_{jets}(E_{\mathrm{clusters}} + E_{\mathrm{track}}) \leq 0.6 E_{CM}$ if both jets originate from μ's.	
	Jets originating from μ's satisfy at least one of the following: $N^{MB}_{\mathrm{layers}} \geq 2$ $E^{\mathrm{charged}}_{\mathrm{clusters}} < 2$ GeV $N^{HCAL}_{\mathrm{layers}} \geq 4$ $N^{HCAL}_{\mathrm{outer\ 3\ layers}} \geq 1$ $N^{HCAL}_{\mathrm{hits/layer}} < 2.0$	N^{MB}_{layers}: number of layers in MB with signals associated to the jet. $E^{\mathrm{charged}}_{\mathrm{clusters}}$: energy of cluster associated to the charged track. $N^{HCAL}_{\mathrm{layers}}$: number of HCAL layers with signals associated to the track. $N^{HCAL}_{\mathrm{outer\ 3\ layers}}$: number of layers hit in the outer HCAL. $N^{HCAL}_{\mathrm{hits/layer}}$: average number of hits per layer for the whole jet.
$e^+e^- \to q\bar{q}$ rejection	$2 \leq N_{\mathrm{tracks}} \leq 8$ $N_{\mathrm{clusters}} \leq 10$	N_{tracks}: number of good tracks in the event. N_{clusters}: the number of good clusters in the τ pair event.

Table 4.3: The τ selection list of criteria.

	Requirements	Variable definition
Two-photon rejection	$\theta_{\mathrm{acol}} \leq 15°$ and $E_{\mathrm{vis}} \geq 0.03E_{CM}$ and at least one of the following 3: $E_{\mathrm{vis}} > 0.20E_{CM}$ or $E_{\mathrm{ECAL}} > 2.0$ GeV or $E_{\mathrm{CJ}} > 2.0$ GeV	θ_{acol}: the supplement of the angle between the two jets in the τ pair event. E_{vis}: $\sum_{\mathrm{jet}}$ Max $(E_{\mathrm{ECAL}}, E_{\mathrm{CJ}})$. E_{ECAL}: total energy deposited in ECAL clusters. E_{CJ}: total energy deposited in CJ.
Cosmic ray rejection	$|d_0|_{\mathrm{min}} \leq 0.5$ cm $|z_0|_{\mathrm{min}} \leq 20.0$ cm $|z_0|_{\mathrm{average}} \leq 20.0$ cm $|t_{\mathrm{meas}} - t_{\mathrm{exp}}| \leq 10$ ns for at least one TOF counter. $|t_{\mathrm{i}} - t_{\mathrm{j}}| < 10$ ns for some TOF counters i and j with $|\phi_i - \phi_j| \geq 165°$.	$|d_0|_{\mathrm{min}}$: minimum $|d_0|$ of all tracks. $|z_0|_{\mathrm{min}}$: minimum $|z_0|$ of all tracks. $|z_0|_{\mathrm{average}}$: average $|z_0|$ of all tracks. $|t_{\mathrm{meas}} - t_{\mathrm{exp}}|$: measured - expected TOF. $|t_{\mathrm{i}} - t_{\mathrm{j}}|$: TOF difference for 2 opposite counters.

Table 4.4: The τ selection list of criteria (continued).

Background	Contamination (%)
$e^+e^- \rightarrow q\bar{q}$	0.74 ± 0.05
$e^+e^- \rightarrow \mu^+\mu^-$	0.72 ± 0.05
$e^+e^- \rightarrow e^+e^-$	0.41 ± 0.07
$e^+e^- \rightarrow (e^+e^-)e^+e^-$	0.07 ± 0.02
$e^+e^- \rightarrow (e^+e^-)\mu^+\mu^-$	0.08 ± 0.02
Total	2.02 ± 0.10

Table 4.5: Non-τ background in the $\tau^+\tau^-$ sample.

Chapter 5

Selection of $\tau^- \longrightarrow 3\mathrm{h}^- 2\mathrm{h}^+ (\geq 0\pi^0)\nu_\tau$ Jets

This chapter describes the selection of $\tau^- \longrightarrow 3\mathrm{h}^- 2\mathrm{h}^+ (\geq 0\pi^0)\nu_\tau$ (5-prong) events, which is applied to the $e^+e^- \to \tau^+\tau^-$ sample described in Chapter 4.

The first requirement is that one of the jets in the event has five good charged tracks, and that the sum of the charges conserves the τ charge. There are 1668 jets in the data sample that meet this requirement. The Monte Carlo simulation predicts that approximately 70 percent of the 5-prong decays pass these requirements. In the other 30 percent of the 5-prong jets, two tracks may fail to be resolved resulting in a 5-prong jet having four tracks. In addition, the conversion of a photon to an e^+e^- pair or the interaction of one of the hadrons can add tracks to the jet.

The Monte Carlo simulation predicts that about 83 percent of the 5-track sample is background. One of the dominant backgrounds is from the $\tau^- \to h^- h^- h^+ \pi^0 \nu_\tau$ decay, which has a branching ratio of 0.045. The π^0 can either decay to two photons, or to a photon and an e^+e^- pair, with branching ratios of 0.988 and 0.012, respectively. In the first case, there is about a 3 percent probability that one of the photons will convert to an e^+e^- pair in the material of the detector, causing this jet to end up in

the 5-track sample. In the second case, the jet goes directly into the 5-track sample. The other dominant background is from $e^+ e^- \to q\bar{q}$ events which were not rejected by the τ pair selection.

The 5-prong selection criteria used to reject these and other types of background events are outlined in Table 5.1. First, we identify and reject jets which include photon conversions. Next, we reject jets in which there is a secondary vertex, i.e. where a pair of tracks appears to originate from a position away from the $e^+ e^-$ or primary vertex. Finally, a set of requirements is applied in order to remove the residual background.

Criterion	Description
	Select 5-track jets:
1	$N_{tracks} = 5$ ($\sum q = \pm 1$)
	Select $\tau^- \longrightarrow 3\text{h}^- 2\text{h}^+ (\geq 0\pi^0)\nu_\tau$ jets:
2	Photon conversion rejection
3	Rejection based on secondary vertices
4	Electron rejection using $\frac{dE}{dx}$
5	$M_{jet} \leq 2.6$ GeV
6	$N_{clusters}^{ECAL} \leq 8$
7	$\frac{E}{P} \leq 0.8$

Table 5.1: Inclusive 5-Prong Selection Criteria

5.1   Photon conversion rejection

Most of the $\tau^- \to h^- h^- h^+ \pi^0 \nu_\tau$ decays can be rejected by identifying jets that have photon conversions. An OPAL photon conversion finder was used to calculate the probability that a given pair of tracks in the jet belongs to an $e^+ e^-$ pair created by

a photon conversion.[25]

The algorithm determines this probability by relying on measurements of the following input quantities:

- the distance between the two tracks at their point of tangency,

- the radius of the first measured hit (in the tracking chambers) of both tracks, and the radius of their common vertex,

- the reconstructed invariant mass of the pair assuming that the two tracks are electron tracks,

- the impact parameter of the reconstructed photon with respect to the primary vertex of the event,

- the momentum of both tracks times the sign of their charge,

- the output from an electron identification algorithm.

Each track in the jet is paired with every other track, and the probability that the pair results from a photon conversion is determined. If any pair of tracks has a photon conversion probability greater than 0.96, then the jet is rejected. Figure 5.1(a) shows the probability for the pair with the highest photon conversion probability in the jet. Events in the final bin of Figure 5.1(a) are rejected by this criterion.

Jets which are identified as having photon conversions have a corresponding secondary vertex. In Figure 5.1(b), the radial distance to the conversion vertex is plotted. The peak at 8.8 cm corresponds to the inner wall of the pressure vessel, and the peak at 23.5 cm corresponds to the boundary between the vertex chamber and the jet chamber.

A total of 1200 jets out of the 1668 jets in the five-track sample are found to contain a photon conversion. After rejecting these jets, the residual sample of 468 jets has a fractional background of 0.64 according to the Monte Carlo simulation.

5.2   Rejection of background decays using a vertex finder

All of the tracks in a 5-prong τ decay nominally originate at the primary vertex. If a pair of tracks originates from a position other than the primary vertex (i.e. a secondary vertex), then the jet is assumed to be background and is rejected from the sample. For example, 3-prong τ decays involving a K^0_s which subsequently decays to a $\pi^+\pi^-$ pair would be rejected by this requirement. In addition, a hadron in a jet may interact with nuclear material in the detector and the particles subsequently produced would appear to come from a secondary vertex.

In criterion three, we use an OPAL vertex finding subroutine [26] to identify pairs of tracks originating from a position other than the primary vertex. The subroutine tags pairs of oppositely-charged tracks which appear to merge or to cross, and identifies the position of the corresponding vertex. If any of the five good tracks in the jet point only to one or more secondary vertices, and not to the primary vertex, then the jet is rejected. Figure 5.2 shows the radial distance from the primary vertex to the secondary vertex for the jets that are rejected by this criterion. All of the other selection criteria in Table 5.1 have been applied. The peak corresponds to the position of the inner wall of the pressure vessel, where particles interact with nuclear material in the detector.
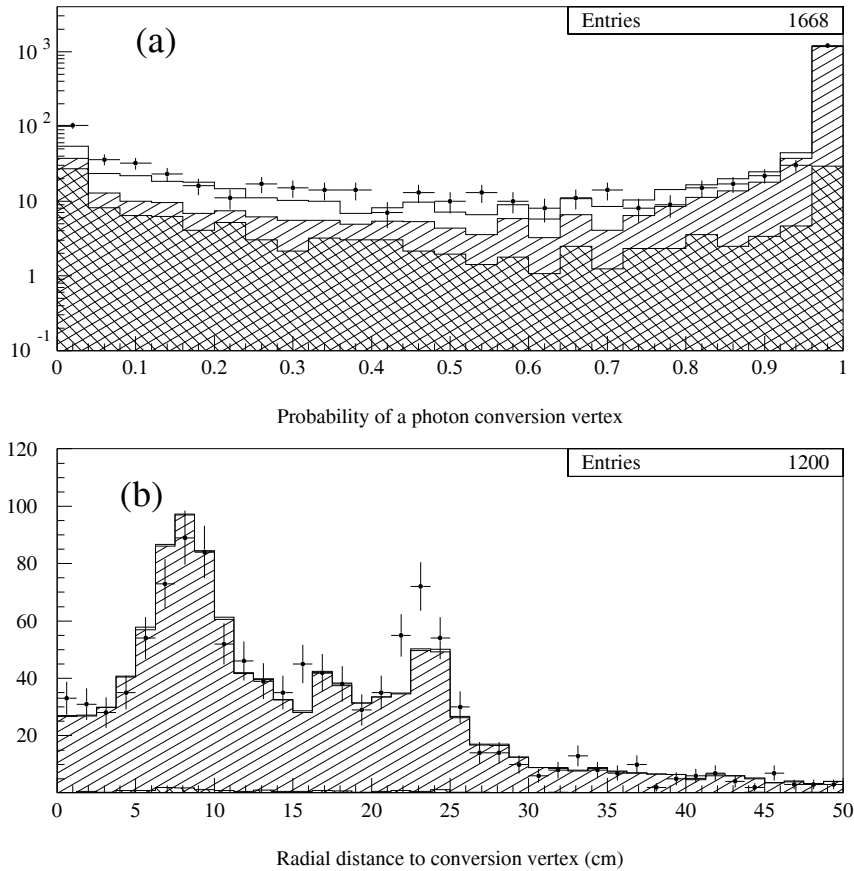
Figure 5.1: (a) The probability for the pair with the highest photon conversion probability, for jets in the five track sample. (b) The radial distance of the photon conversion vertex is plotted for jets with an identified photon conversion. The points are data, the clear histogram is Monte Carlo 5-prong signal prediction, the hatched histogram is Monte Carlo τ background prediction, and the doubly hatched histogram is Monte Carlo $q\bar{q}$ prediction.
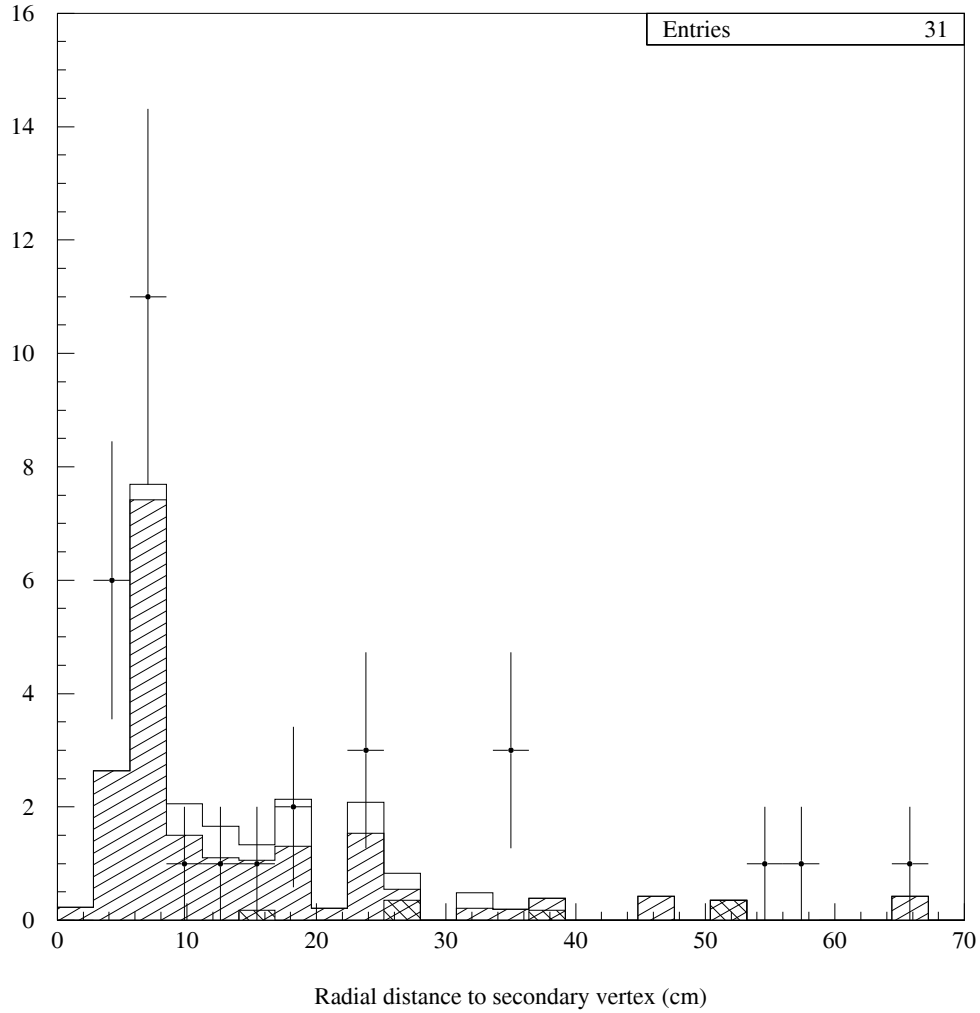
Figure 5.2: The radial distance to the secondary vertices is plotted, for jets with an identified secondary vertex. All of the other criteria in Table 5.1 have been applied. The points are data, the unshaded histogram is Monte Carlo 5-prong signal prediction, the hatched histogram is Monte Carlo τ background prediction, and the doubly hatched histogram is Monte Carlo $q\bar{q}$ prediction.

5.3   Electron rejection using dE/dx

A fraction of the residual background includes photon conversions that were not identified by the algorithm described in Section 5.1. In criterion four, the lowest momentum track is considered to be an electron track if it satisfies ($N_{dE/dx}^{hits} \geq 20$ and $p \leq$ 2 GeV and $\frac{dE}{dx} \geq 9$ keV/cm).

The ability to discriminate between various types of particles using dE/dx is best at low momenta, and so the lowest momentum good track in the jet is used (see Figure 3.3). A reliable $\frac{dE}{dx}$ measurement requires that at least 20 of the 159 wires have good individual measurements or hits, ie: $N_{dE/dx}^{hits} \geq 20$. Figure 5.3 shows the $\frac{dE}{dx}$ of the the lowest momentum track in each jet, where the track has $N_{dE/dx}^{hits} \geq 20$ and $p \leq 2$ GeV.

5.4   Other background rejection criteria

Three additional criteria are applied to further reduce the background in the sample. The mass of the jet is reconstructed using the measured momenta of the five charged particles in the jet chamber, assuming that they are pions. For τ jets, the jet mass should be less than the mass of the τ (1.8 GeV). In criterion four, the jet mass is required to be less than 2.6 GeV. This helps to remove 1- or 3-prong jets which are accompanied by at least one π^0, as well as background from other τ decays and from $q\bar{q}$ events. Figure 5.4 shows the reconstructed jet mass for jets which satisfy all of the other criteria in Table 5.1.

In criterion six, the number of clusters in the electromagnetic calorimeter is restricted to be fewer than or equal to eight. This reduces the background caused by $q\bar{q}$ events which typically have more clusters (see Figure 5.5).
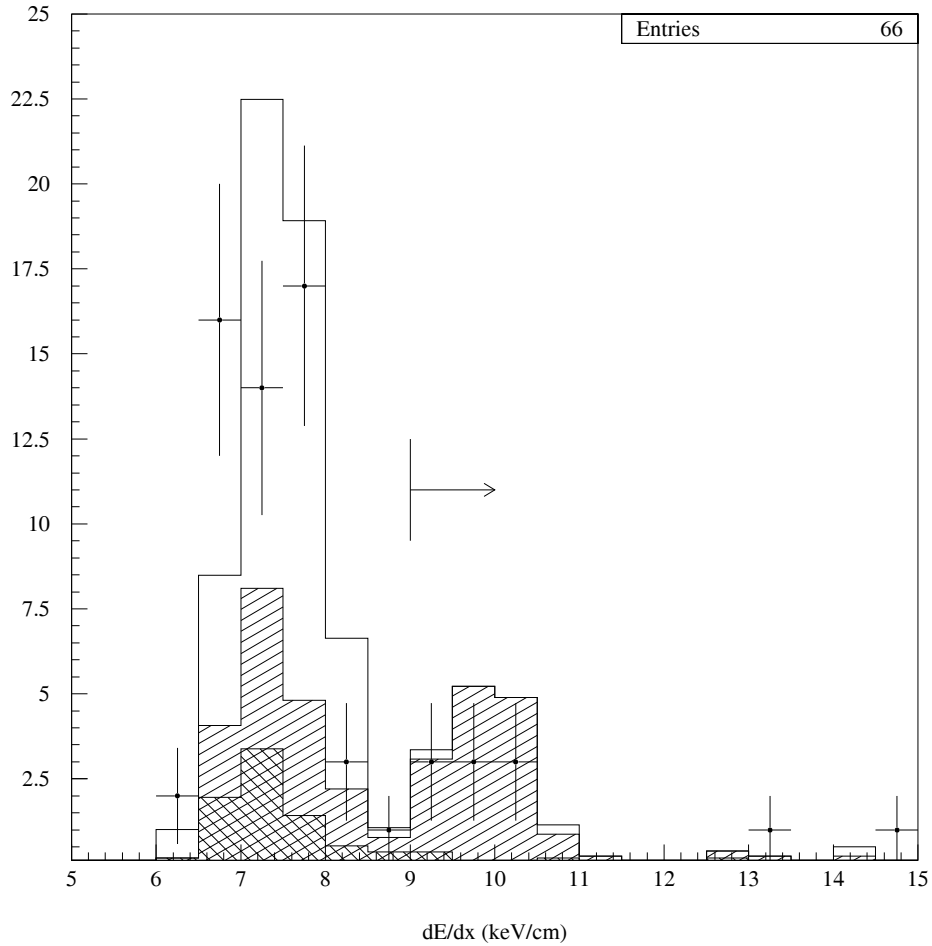
Figure 5.3: $\frac{dE}{dx}$ of the lowest momentum track, where the track has $p \leq 2$ GeV and $N^{hits}_{dE/dx} \geq 20$ for jets which have passed all of the other criteria in Table 5.1. The points are data, the unshaded histogram is Monte Carlo 5-prong signal prediction, the hatched histogram is Monte Carlo τ background prediction, and the doubly hatched histogram is Monte Carlo $q\bar{q}$ prediction. The arrow indicates jets which are rejected by the $\frac{dE}{dx}$ requirement.
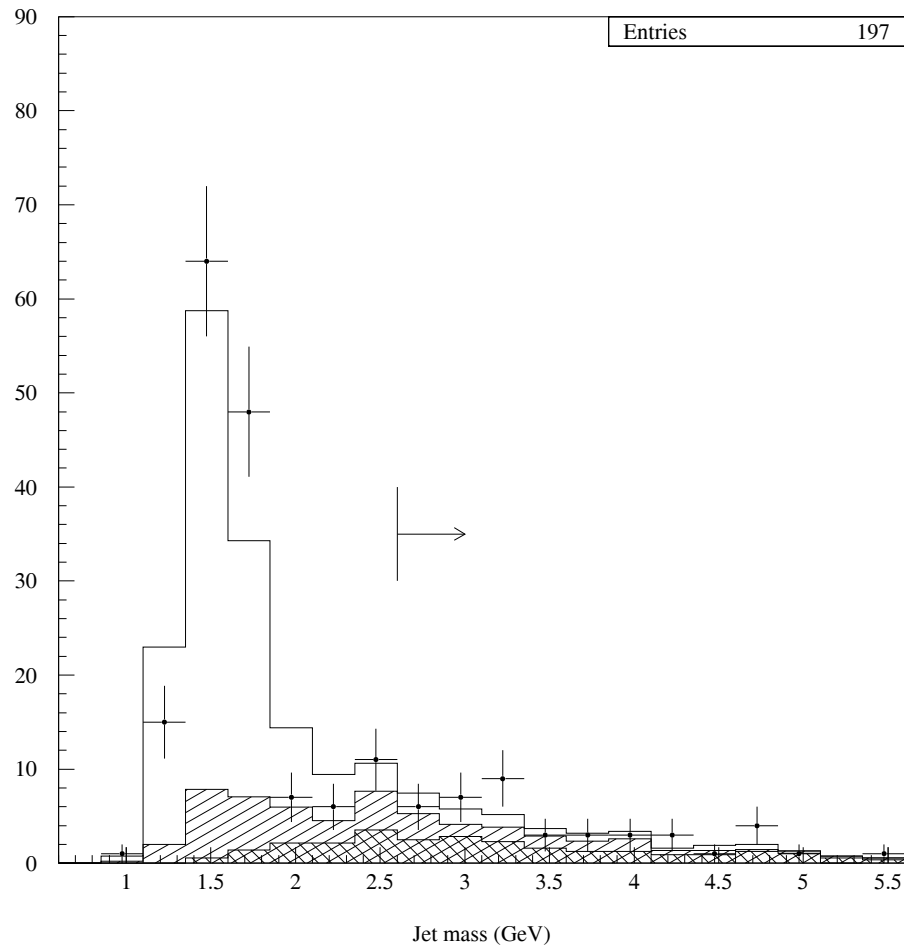
Figure 5.4: The invariant mass of jets which satisfy all of the other criteria in Table 5.1. The points are data, the unshaded histogram is Monte Carlo 5-prong signal prediction, the hatched histogram is Monte Carlo τ background prediction, and the doubly hatched histogram is Monte Carlo $q\bar{q}$ prediction. The arrow indicates jets which are rejected by the mass requirement.
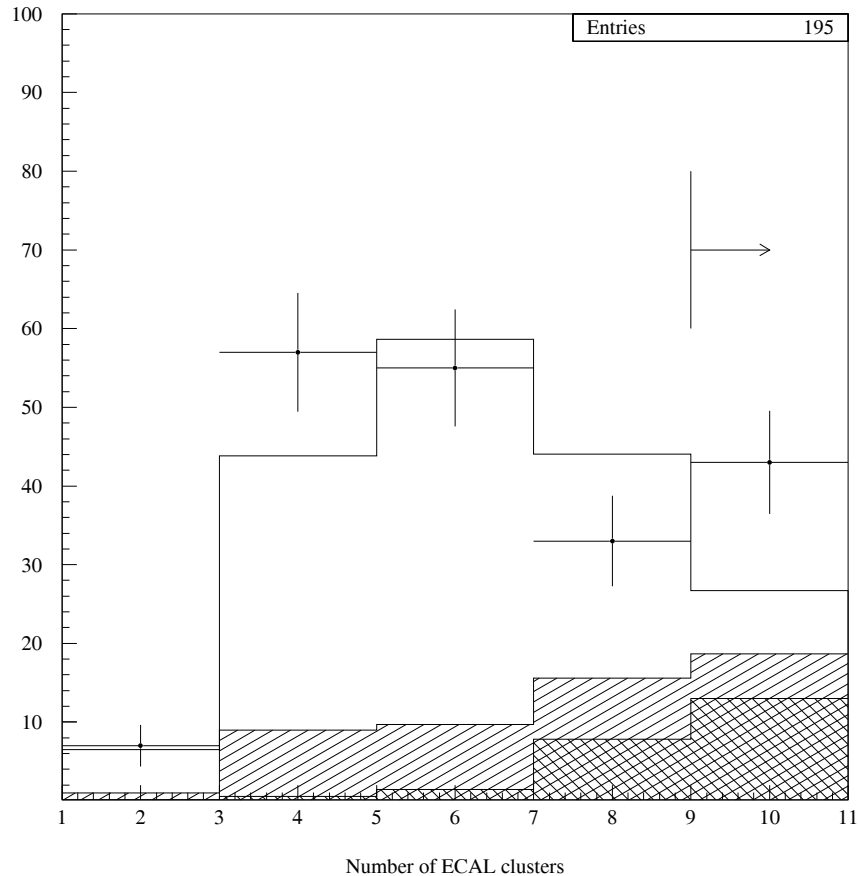
Figure 5.5: The number of ECAL clusters for jets which have passed all of the other criteria in Table 5.1. The points are data, the unshaded histogram is Monte Carlo 5-prong signal prediction, the hatched histogram is Monte Carlo τ background prediction, and the doubly hatched histogram is Monte Carlo $q\bar{q}$ prediction. The arrow indicates the jets which are rejected by the requirement on the number of clusters.

Decay Channel	f_{bkgd}
$(3\pi)^- \pi^0$	0.105
$(3\pi)^-$	0.034
Other τ decays	0.020
$q\bar{q}$	0.055
Total	0.214

Table 5.2: Fractional Background in the 5-prong Sample

A pion loses about 30 percent of its energy in the electromagnetic calorimeter. Thus, for jets containing only pions, one expects the following:

$$\frac{E}{P} \equiv \sum_{jet} E_{cluster} / \sum_{jet} |\vec{p}_i| \approx 0.3, \tag{5.1}$$

where $\sum_{jet} E_{cluster}$ is the energy measured in the electromagnetic calorimeter from clusters which have a corresponding track in the jet chamber, and $\sum_{jet} |\vec{p}_i|$ is the total scalar momentum measured for the five charged particles. Jets containing photons or electrons, which deposit all of their energy in the electromagnetic calorimeter, have a higher $\frac{E}{P}$ than jets which contain only charged pions. By requiring $\frac{E}{P} \leq 0.8$, criterion seven screens out jets which contain extra photons, thus reducing the background due to τ decays in which a photon has converted (see Figure 5.6).

5.5 Results of the $\tau^- \longrightarrow 3h^- 2h^+ (\geq 0\pi^0)\nu_\tau$ Selection

The selection yields a sample of 152 5-prong candidates, with an efficiency of 0.52 and a fractional background of 0.21 as estimated by the Monte Carlo simulation. The main types of background are presented in Table 5.2. The error on the background will be discussed in Chapter 6.
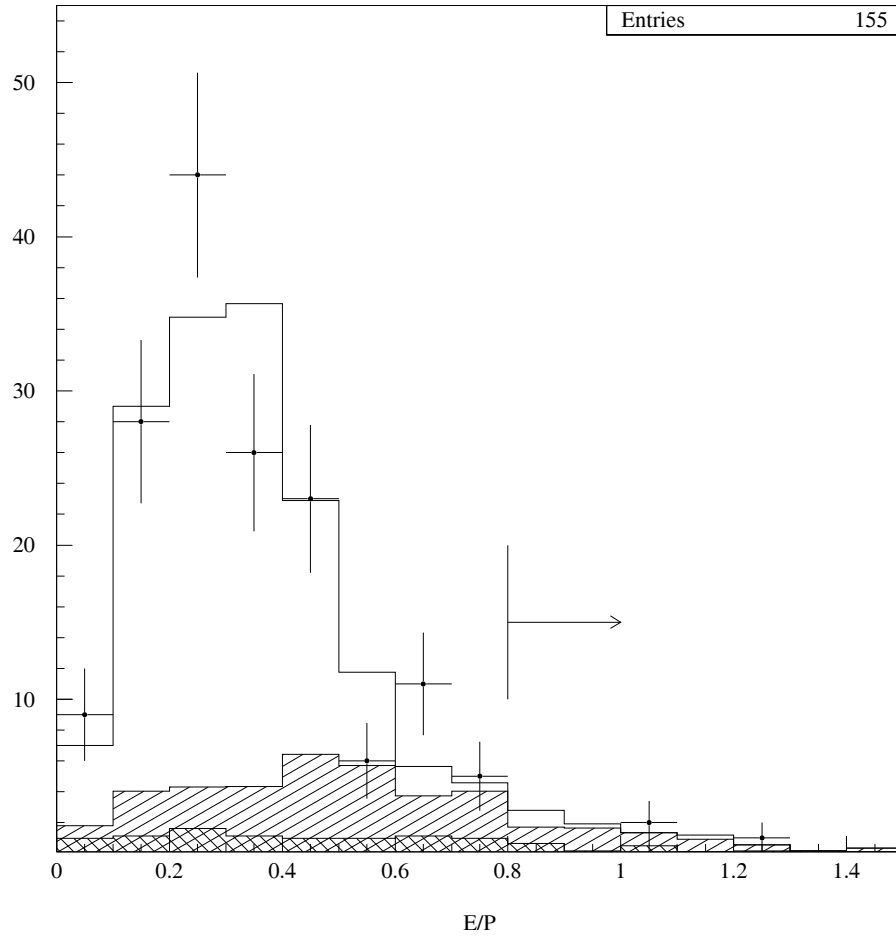
Figure 5.6: $\frac{E}{P}$ for jets which have met all of the other criteria in Table 5.1. The points are data, the unshaded histogram is Monte Carlo 5-prong signal prediction, the hatched histogram is Monte Carlo τ background prediction, and the doubly hatched histogram is Monte Carlo $q\bar{q}$ prediction. The arrow indicates jets which are rejected by the $\frac{E}{P}$ requirement.

Chapter 6

The 5-Prong Branching Ratio

The 5-prong branching ratio, $\mathrm{B}(\tau^- \longrightarrow 3\mathrm{h}^- 2\mathrm{h}^+ (\geq 0\pi^0)\nu_\tau)$, is defined to be the number of τ particles, N_{5p}, which decay via the $\tau^- \longrightarrow 3\mathrm{h}^- 2\mathrm{h}^+ (\geq 0\pi^0)\nu_\tau$ decay mode, divided by the total number of τ particles, N_τ, and can be written

$$B = \frac{N_{5p}}{N_\tau}. \tag{6.1}$$

The $\tau^+ \tau^-$ sample includes a small fraction of background. Therefore, the true number of τ's in the sample, N_τ, is

$$N_\tau = N_\tau^{obs}(1 - f_{non-\tau}) \tag{6.2}$$

where N_τ^{obs} is the number of τ candidates, and $f_{non-\tau}$ is the fractional background in the τ sample.

The 5-prong selection process removes some $\tau^- \longrightarrow 3\mathrm{h}^- 2\mathrm{h}^+ (\geq 0\pi^0)\nu_\tau$ jets, and also allows some background jets into the sample. Thus, the true number of signal jets, N_{5p}, is

$$N_{5p} = \frac{N_{5p}^{obs}}{\epsilon_{5p}}(1 - f_{bkgd}) \tag{6.3}$$

where

- N_{5p}^{obs} is the number of observed $\tau^- \longrightarrow 3\mathrm{h}^- 2\mathrm{h}^+ (\geq 0\pi^0)\nu_\tau$ candidates passing the selection,

- ϵ_{5p} is the efficiency for selecting the $\tau^- \longrightarrow 3h^- 2h^+ (\geq 0\pi^0)\nu_\tau$ candidates,

- f_{bkgd} is the fractional background in the sample.

The efficiency and background are determined by the Monte Carlo simulations.

The τ pair selection does not select all modes of τ decay equally well, and therefore introduces a bias into the measured value of $B(\tau^- \longrightarrow 3h^- 2h^+ (\geq 0\pi^0)\nu_\tau)$. The bias factor, F_{bias}, is determined using the Monte Carlo simulation, and is defined as the ratio

$$F_{bias} = \frac{B(\tau^- \longrightarrow 3h^- 2h^+ (\geq 0\pi^0)\nu_\tau)^{before}}{B(\tau^- \longrightarrow 3h^- 2h^+ (\geq 0\pi^0)\nu_\tau)^{after}}$$

where *before* and *after* refer to the τ selection process.

The branching ratio is determined by combining Equations 6.1, 6.2, 6.3, and including the τ pair selection bias to give:

$$B = \frac{N_{5p}^{obs}(1 - f_{bkgd})}{N_\tau^{obs}(1 - f_{non-\tau})} \frac{1}{\epsilon_{5p}} \frac{1}{F_{bias}}. \tag{6.4}$$

The background, f_{bkgd}, can be determined directly from the Monte Carlo simulations, in which case

$$f_{bkgd} = \frac{\sum_{i=1}^{n_{bg}} N_i^{mc} + N_q^{mc}}{N_{5p}^{mc} + \sum_{i=1}^{n_{bg}} N_i^{mc} + N_q^{mc}} \tag{6.5}$$

where

- n_{bg} is the number of background decay channels used in the Monte Carlo simulation,

- N_i^{mc} is the number of Monte Carlo candidates for the ith background decay channel passing the selection,

- N_q^{mc} is the number of Monte Carlo $q\bar{q}$ candidates passing the selection,

- N_{5p}^{mc} is the number of Monte Carlo $\tau^- \longrightarrow 3h^- 2h^+ (\geq 0\pi^0)\nu_\tau$ candidates passing the selection.

Alternatively, the background can be written as

$$f_{bkgd} = \frac{\sum_{i=1}^{n_{bg}} \epsilon_i B_i + \frac{N_q^{mc}}{N_\tau^{mc}}}{\epsilon_{5p} B + \sum_{i=1}^{n_{bg}} \epsilon_i B_i + \frac{N_q^{mc}}{N_\tau^{mc}}} \tag{6.6}$$

which can be derived using the following definitions:

- $\epsilon_i \equiv \frac{N_i^{mc}}{N_i^{init-mc}}$ is the efficiency for decays of the ith type passing the selection, where $N_i^{init-mc}$ is the (initial) number of decays of the ith type,

- N_τ^{mc} is the number of τ particles in the Monte Carlo sample after the τ selection,

- $B_i \equiv \frac{N_i^{init-mc}}{N_\tau^{mc}}$ is the branching ratio of the ith background decay channel.

Each of the branching ratios in Equation 6.6 must be modified by the τ selection bias factor for that mode of decay; however, for all but the 5-prong branching ratio, the bias factor is very close to unity and can be neglected. The expression for the background then becomes

$$f_{bkgd} = \frac{\sum_{i=1}^{n_{bg}} \epsilon_i B_i + \frac{N_q^{mc}}{N_\tau^{mc}}}{\epsilon_{5p} B F_{bias} + \sum_{i=1}^{n_{bg}} \epsilon_i B_i + \frac{N_q^{mc}}{N_\tau^{mc}}} . \tag{6.7}$$

Using Equation 6.7 to replace f_{bkgd} in Equation 6.4, one finds that B appears on both sides of the equation. Solving for B yields

$$B = \frac{K - \sum_{i=1}^{n_{bg}} \epsilon_i B_i - \frac{N_q^{mc}}{N_\tau^{mc}}}{\epsilon_{5p} F_{bias}} \tag{6.8}$$

where

$$K \equiv \frac{N_{5p}^{obs}}{N_\tau^{obs}(1 - f_{non-\tau})}$$

and other parameters are as defined above.

6.1   Results

The τ 5-prong branching ratio, $B(\tau^- \longrightarrow 3\mathrm{h}^- 2\mathrm{h}^+ (\geq 0\pi^0)\nu_\tau)$, is determined using Equation 6.8 with the parameters listed in Table 6.1, and is found to be

$$B(\tau^- \longrightarrow 3\mathrm{h}^- 2\mathrm{h}^+ (\geq 0\pi^0)\nu_\tau) = (1.25 \pm 0.14 \pm 0.08) \times 10^{-3}$$

where the first error is statistical and the second is systematic.

Parameter	Value
N_{5p}^{obs}	152
N_{τ}^{obs}	196694
$f_{non-\tau}$	0.020 ± 0.001
F_{bias}	0.94 ± 0.01
ϵ_{5p}	0.521 ± 0.017
B	$(1.25 \pm 0.14 \pm 0.08) \times 10^{-3}$

Table 6.1: Branching Ratio Parameters for $B(\tau^- \longrightarrow 3\mathrm{h}^- 2\mathrm{h}^+ (\geq 0\pi^0)\nu_\tau)$

The statistical error includes components based on the total number of data events, the predicted number $\tau^+ \tau^-$ background events, and the predicted number of $q\bar{q}$ events.

The systematic uncertainty (see Table 6.2) includes the uncertainty in the $q\overline{q}$ background, and the error in the 5-prong efficiency due to the limited size of the Monte Carlo sample. It also includes the uncertainty in the τ background channels, the error in the branching ratios of the background modes of τ decay, and the errors in $f_{non-\tau}$ and F_{bias}.

The uncertainty in the $q\overline{q}$ and τ backgrounds was investigated using a sample of four-track jets. The composition of this sample (3-prong τ decays with a photon conversion, and $q\overline{q}$ events) is very similar to the background found in the five-track sample. In Figure 6.1(a), the mass of the jets in this sample are plotted. The jets

Variable	Error ($\times 10^{-3}$)
$q\overline{q}$ background	0.049
Efficiency	0.042
$\tau^+\tau^-$ background	0.036
Bias factor	0.013
non-τ background	0.002
Total	0.075

Table 6.2: Systematic Uncertainties

were required to satisfy the photon conversion, secondary vertices, number of ECAL clusters, and E/P requirements (numbers 2, 3, 6, and 7) in Table 5.1. The mass distributions for the τ and $q\overline{q}$ jets are different. As a result, the modelling of the background can be checked by simultaneously fitting the normalization of the τ and $q\overline{q}$ distributions to the data shown in Figure 6.1(a). The results of the fit are found to be 1.03 ± 0.14 for the τ distribution, and 0.43 ± 0.22 for the $q\overline{q}$ distribution, and are shown in Figure 6.1(b). Although the normalization factor obtained for the $q\overline{q}$ background is significantly less than unity, it has been noted in other OPAL analyses [27] that the $q\overline{q}$ Monte Carlo simulation gives more low multiplicity events than observed in the data. The errors from the fit are included in the systematic uncertainties of the τ and $q\overline{q}$ backgrounds (see Table 6.2).

As a further cross-check, the criteria applied to the variables in the 5-prong selection were varied. The resulting variations in the branching ratio were found to be consistent with the quoted uncertainty, and are presented in Table 6.3.
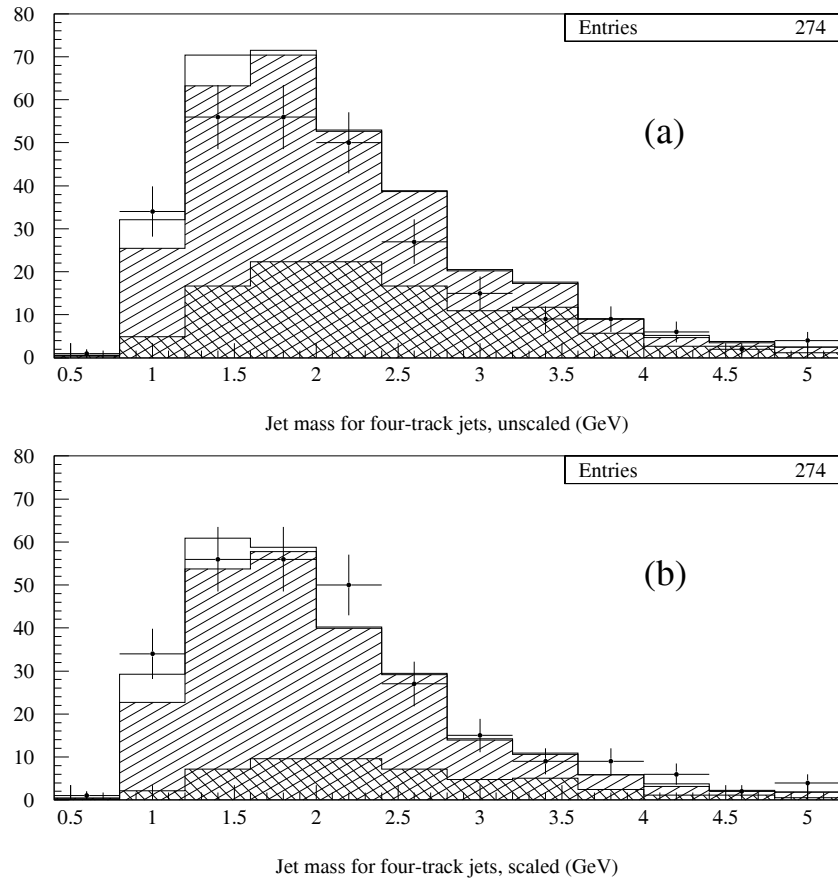
Figure 6.1: (a) The unscaled four-track sample, with criteria 2, 3, 6,and 7 from Table 5.1 applied. (b) The scaled four-track sample, with the same criteria applied as in (a). The points are data, the clear histogram is Monte Carlo 5-prong signal prediction, the hatched histogram is Monte Carlo τ background prediction, and the doubly hatched histogram is Monte Carlo $q\overline{q}$ prediction.

Variable	Range of cut	Range of branching ratio ($\times 10^{-3}$)
M_{jet}	2.4 - 3.2 GeV	1.21 - 1.26
E/P	0.6 - 0.9	1.18 - 1.25
$N^{ECAL}_{clusters}$	7 - 9	1.25 - 1.33
dE/dx	8.4 - 9.2 keV/cm	1.25

Table 6.3: Results of Variation of Criteria

Chapter 7

Conclusions

The branching ratio of the $\tau^- \longrightarrow 3\mathrm{h}^-2\mathrm{h}^+(\geq 0\pi^0)\nu_\tau$ decay has been measured using OPAL data from 1991 through 1995, and is found to be

$$B(\tau^- \longrightarrow 3\mathrm{h}^-2\mathrm{h}^+(\geq 0\pi^0)\nu_\tau) = (1.25 \pm 0.14 \pm 0.08) \times 10^{-3},$$

where the first error is statistical and the second is systematic. Figure 7.1 shows how this value compares with previous measurements from other experiments, as given in the Particle Data Book [1]. The solid band is the Particle Data Group fit of the measurements from the various experiments. The ALEPH result shown on the figure was obtained by adding the branching ratios for the two exclusive modes of decay, $\tau \to 3h^-2h^+\nu_\tau$, and $\tau \to 3h^-2h^+\pi^0\nu_\tau$, and adding the errors in quadrature [28]. The branching ratio measured in this work is consistent with previous measurements, although it is significantly lower than the previous OPAL measurement which was based on 1991 and 1992 data [29].

The results from this work have been used as the basis for an OPAL publication [27], in which measurements of the branching ratios for the two exclusive τ 5-prong modes of decay are presented, as well as the branching ratio for the inclusive mode measured here. In addition, an upper limit on the τ neutrino mass has been measured
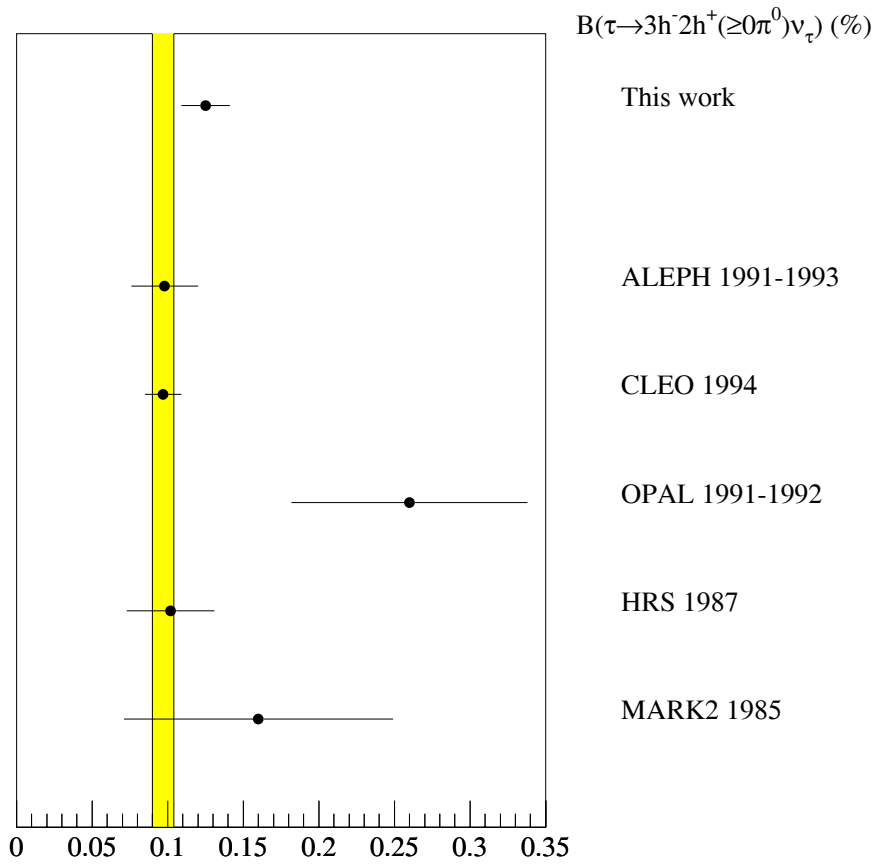
Figure 7.1: Measurements of $B(\tau^- \longrightarrow 3h^-2h^+(\geq 0\pi^0)\nu_\tau)$ are plotted with uncertainties. The solid band is the Particle Data Group fit to the data.

to be less than 27.6 MeV using OPAL data from 1990 to 1995, and a 5-prong sample produced by a selection not unlike the one presented here [4].

Bibliography

[1] Caso, C. *et al.*, Particle Data Group, European Physical Journal **C3** (1998) 1.

[2] Bai, J. *et al.*, BES Collaboration, Phys. Rev. **D53** (1996) 20.

[3] Fukuda, Y. *et al.*, Super-Kamiokande Collaboration, *Study of the Atmospheric Neutrino Flux in the Multi-GeV Energy Range*, ICRR-REPORT-418-98, hep-ex/9805006, preprint, May 1998 14pp.

[4] Ackerstaff, K. *et al.*, OPAL Collaboration, *An Upper Limit for the τ Neutrino Mass from $\tau \to 5\pi^{\pm}\nu_{\tau}$ Decays*, CERN-EP/98-055, preprint, 15th April, 1998.

[5] Böhm, F. and Vogel, P. *Physics of Massive Neutrinos*, Cambridge Univ. Press (1987).

[6] Glashow,S., Nucl. Phys. **22** (1961) 579.
Weinberg, S., Phys. Rev. Lett., **19** (1967) 1264.
Salam, A. *Elementary Particle Theory*, ed. N. Svartholm., Almquist and Wiksell, Stockholm (1968).

[7] Perl, M., Rep. Prog. Phys. **55** (1992) 653.

[8] Kühn, J. and Santamaria, A., Z. Phys. **C48** (1990) 445.

[9] Isgur, N., Morningstar, C., and Reader, C., Phys. Rev. **D39** (1989) 1357.

[10] Ackerstaff, K. *et al.*, OPAL Collaboration, *A Measurement of the Hadronic Decay Current and the ν_{τ}-Helicity in $\tau \to \pi^{-}\pi^{-}\pi^{+}\nu_{\tau}$*, CERN-PPE/97-020, preprint, 21st February 1997.

[11] Pham, T. *et al*, Phys. Lett. **78B** (1978) 623.

[12] Tsai, Y., Phys. Rev. **D4** (1971) 2821.

[13] Eidelman, S. and Ivanchenko, V., Nucl. Phys. B (Proc. Suppl.) **55C** (1997) 181.

[14] Ahmet, K. *et al*, OPAL Collaboration, Nuclear Inst. and Methods **A 305** (1991) 275.

[15] Allport, P. *et al.*, OPAL Collaboration, Nuclear Inst. and Methods **A 324** (1993) 34.

[16] Anderson, S. *et al.*, OPAL Collaboration, Nuclear Inst. and Methods **A 403**, (1998) 326.

[17] Jadach S., Ward B., and Was Z., Comp. Phys. Comm. **79** (1994) 503.

[18] Decker R., Jadach S., Kühn J., and Was Z., Comp. Phys. Comm. **76** (1993) 361.

[19] Allison J. *et al.*, Nucl. Instr. and Meth. **A 317** (1992) 47.

[20] Brun R. *et al.*, GEANT 3, Report DD/EE/84-1 CERN (1989).

[21] Sjostrand, T., *PYTHIA 5.7 and JETSET 7.4: Physics and Manual*, CERN-TH-7112-93 (1994) 305.

[22] Marchesini, G. *et al.*, Comput. Phys. Commun. **67** (1992) 465.

[23] Sasaki, M. *et al.*, OPAL Collaboration, $\tau\bar{\tau}$ *Selection*, Internal Document.

[24] Sobie, R. and Stumpf, L., *A Measurement of the Branching Ratios of the Decay of the τ Lepton to Five Charged Hadrons*, OPAL TN529 (1998).

[25] Lafoux, H., *A Neural Conversion Finder*, OPAL TN290 (1995).

[26] Akers, R. *et al.*, OPAL Collaboration, Phys. Lett. **339** (1994) 278.

[27] Ackerstaff, K. *et al.*, OPAL Collaboration, CERN-EP/98-090, preprint June 3rd, 1998.

[28] Buskulic, D. *et al.*, ALEPH Collaboration, Z. Phys. **C70** (1996) 579.

[29] Acton, P.D. *et al.*, OPAL Collaboration, Phys. Lett. **288B** (1992) 373.

Vita

Surname:	Stumpf
Given Names:	Laura
Place of Birth:	Yorkton, Saskatchewan, Canada
Date of Birth:	24th of September, 1959

Educational Institutions Attended:

Malaspina College, Canada	1991-1992
University of Victoria, Canada	1992-1998

Degrees Awarded:

Hon. B.Sc. (Physics) University of Victoria, Canada	1996

Honours and Awards:

NSERC Summer Scholarship	1995
NSERC PGSA Award	1996

Publications:

The OPAL Collaboration, K. Ackerstaff *et al.*,
Measurement of the Tau Branching Ratios to Five Charged Hadrons,
CERN-EP/98-090, June 1998. 13pp. submitted to the European Phys. Journal

Partial Copyright License

I hereby grant the right to lend my thesis to users of the University of Victoria Library, and to make single copies only for such users, or in response to a request from the Library of any other university or similar institution, on its behalf or for one of its users. I further agree that permission for extensive copying of this thesis for scholarly purposes may be granted by me or a member of the university designated by me. It is understood that copying or publication of this thesis for financial gain shall not be allowed without my written permission.

Title of Thesis:

A Measurement of the Branching Ratio of the Decay of the τ Lepton to Five Charged Hadrons

Author: Laura Stumpf

_____

_____

September 5, 1998